AD-A076 125 DAVID W TAYLOR NAVAL SHIP RESEARCH AND DEVELOPMENT CE--ETC F/G 9/5
NO-LOAD TESTING OF THE SHAPED FIELD SUPER-CONDUCTIVE MOTOR.(U)
OCT 79 H N ROBEY , M J CANNELL
UNCLASSIFIED DTNSRDC-79/076 NL

1 OF 1
AD A 076125

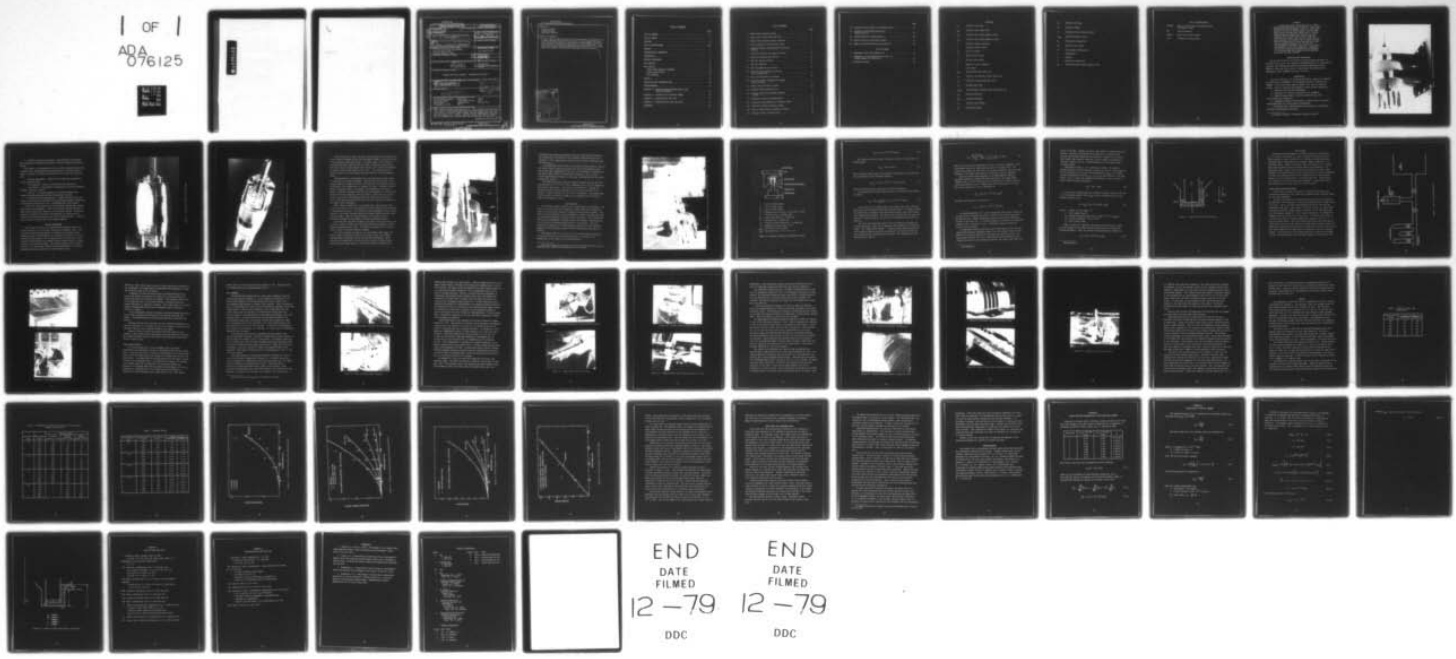

END
DATE FILMED
12-79
DDC

END
DATE FILMED
12-79
DDC

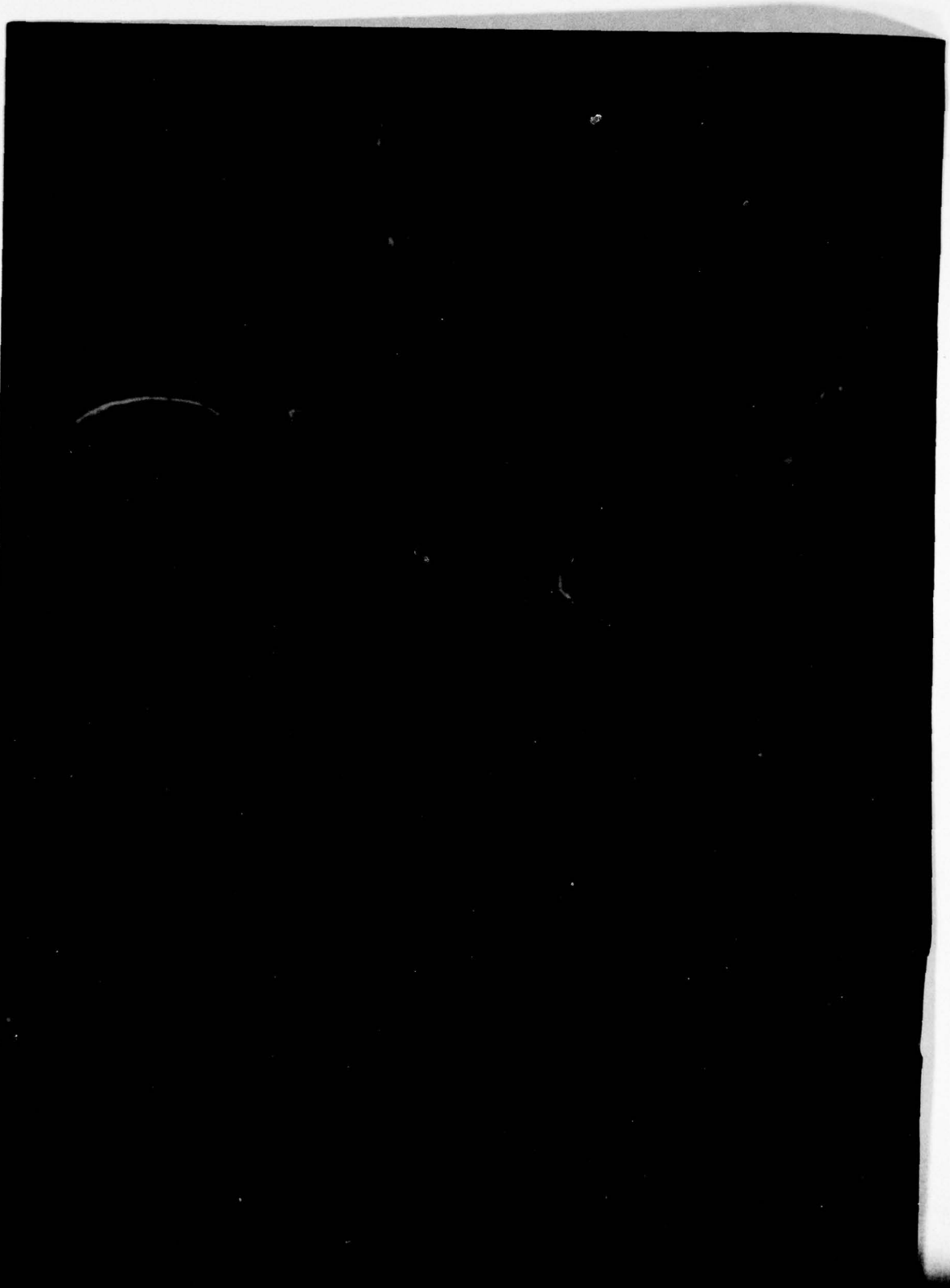

UNCLASSIFIED

SECURITY CLASSIFICATION OF THIS PAGE (When Data Entered)

REPORT DOCUMENTATION PAGE

READ INSTRUCTIONS BEFORE COMPLETING FORM

1. REPORT NUMBER: DTNSRDC-79/076
2. GOVT ACCESSION NO.
3. RECIPIENT'S CATALOG NUMBER
4. TITLE (and Subtitle): NO-LOAD TESTING OF THE SHAPED FIELD SUPER-CONDUCTIVE MOTOR
5. TYPE OF REPORT & PERIOD COVERED: Final, Sept 13
6. PERFORMING ORG. REPORT NUMBER
7. AUTHOR(s): H.N. Robey, M.J. Cannell, L.T. Dunnington
8. CONTRACT OR GRANT NUMBER(s)
9. PERFORMING ORGANIZATION NAME AND ADDRESS: David W. Taylor Naval Ship Research and Development Center, Bethesda, Maryland 20084
10. PROGRAM ELEMENT, PROJECT, TASK AREA & WORK UNIT NUMBERS: (See reverse side)
11. CONTROLLING OFFICE NAME AND ADDRESS
12. REPORT DATE: October 1979
13. NUMBER OF PAGES: 63
14. MONITORING AGENCY NAME & ADDRESS (if different from Controlling Office): 12 55
15. SECURITY CLASS. (of this report): UNCLASSIFIED
15a. DECLASSIFICATION/DOWNGRADING SCHEDULE
16. DISTRIBUTION STATEMENT (of this Report)

APPROVED FOR PUBLIC RELEASE: DISTRIBUTION UNLIMITED

17. DISTRIBUTION STATEMENT (of the abstract entered in Block 20, if different from Report): 16 S038052

18. SUPPLEMENTARY NOTES: 17 S038052

19. KEY WORDS (Continue on reverse side if necessary and identify by block number)

Super Conducting Magnet	Drum Rotors	Stator
Solenoidal Magnet	Liquid Metal Brushes	NaK
Helium Dewar	Refrigeration	No-Load Test
Ferromagnetic Shield	Rotor	

20. ABSTRACT (Continue on reverse side if necessary and identify by block number)

A laboratory-model superconductive d.c. motor, designed and constructed at the David W. Taylor Naval Ship Research and Development Center for peak power output in the 400 to 1000 hp range, has been undergoing no-load testing since January 1973. Results, reported herein, substantially validate the loss estimates (6.5 kW total power loss at 1800 rpm, 120 amp field

(Continued on reverse side)

DD FORM 1 JAN 73 1473 EDITION OF 1 NOV 65 IS OBSOLETE S/N 0102-014-6601

UNCLASSIFIED

SECURITY CLASSIFICATION OF THIS PAGE (When Data Entered)

387 682

(Block 10)

Project S0380-SL
Task Area 16761
Work Unit 2722-100

(Block 20 continued)

current, open circuit) predicted in a prior analysis, and indicate that no major problems should be encountered in future planned load tests, with the possible exception of the collector electromagnetic stability, which cannot be evaluated satisfactorily at no-load conditions. Background information on machine development and discussions of the liquid metal and cryogenic helium handling procedures are also included.

TABLE OF CONTENTS

LIST OF FIGURES

LIST OF TABLES

NOTATION

A_c	Collector site area
A_{dw}	Collector disk wetted area
B_{ca}	Collector site axial magnetic field
B_{cr}	Collector site radial magnetic field
d	Collector radial clearance
f	Fanning friction factor
I_{ej}	Ejection current
I_f	Magnet field current
I_l	Machine load current
N	Number of rotor conductors
n	Rotor speed
P_{cbs}	Bearings and seals power loss
P_{cc}	Collector circulating current power loss
P_{cv}	Collector viscous drag power loss
P_{cw}	Windage power loss
P_{cwbs}	Total windage, bearings, and seals power loss
P_{ej}	Ejection pressure
P_{res}	Restoring pressure
R_c	Collector site radius
R_o	Fluid mean radius

R_{Ω}	Machine resistance
V_T	Terminal voltage
V_c	Average collector fluid velocity
V_{emf}	Back electromotive force
V_{Ω}	Resistance voltage drop
W_c	Collector site width
Δh	Fluid height differential
μ	Permeability
ρ	Density
σ	Electrical resistivity
Φ_E	Average effective radial magnetic flux

LIST OF ABBREVIATIONS

DTNSRDC	David W. Taylor Naval Ship Research and Development Center
NaK	Sodium-Potassium
NAVSEA	Naval Sea Systems Command
TRIM	Triangular Irregular Mesh

ABSTRACT

A laboratory-model superconductive d.c. motor, designed and constructed at the David W. Taylor Naval Ship Research and Development Center for peak power output in the 400 to 1000 hp range, has been undergoing no-load testing since January 1973. Results, reported herein, substantially validate the loss estimates (6.5 kW total power loss at 1800 rpm, 120 amp field current, open circuit) predicted in a prior analysis, and indicate that no major problems should be encountered in future planned load tests, with the possible exception of the collector electromagnetic stability, which cannot be evaluated satisfactorily at no-load conditions. Background information on machine development and discussions of the liquid metal and cryogenic helium handling procedures are also included.

ADMINISTRATIVE INFORMATION

The no-load testing of the shaped field superconducting motor, described in this report, was sponsored by NAVSEA 0331H, Mr. A. Chaikin, and conducted under NAVSEA Superconductive Propulsion Machinery Project S0380-SL, Task Area 16761, David W. Taylor Naval Ship Research and Development Center (DTNSRDC) Work Unit 2722-100.

INTRODUCTION

The 400 to 1000 hp, d.c. superconducting motor (Figure 1), designed and constructed at DTNSRDC,[1*] is undergoing laboratory evaluation at DTNSRDC. The no-load tests began in January 1973, and are reported herein. The test sequences were designed to meet several objectives:

1. Establish motor no-load performance
2. Establish the accuracy of predicted loss estimates
3. Identify design and/or construction deficiencies, and their causes and consequences
4. Determine necessary modifications to motor and/or to improved design approaches for future machine developments
5. Determine areas requiring additional attention in subsequent laboratory and shipboard evaluation

---

*A complete listing of references is given on page 53.

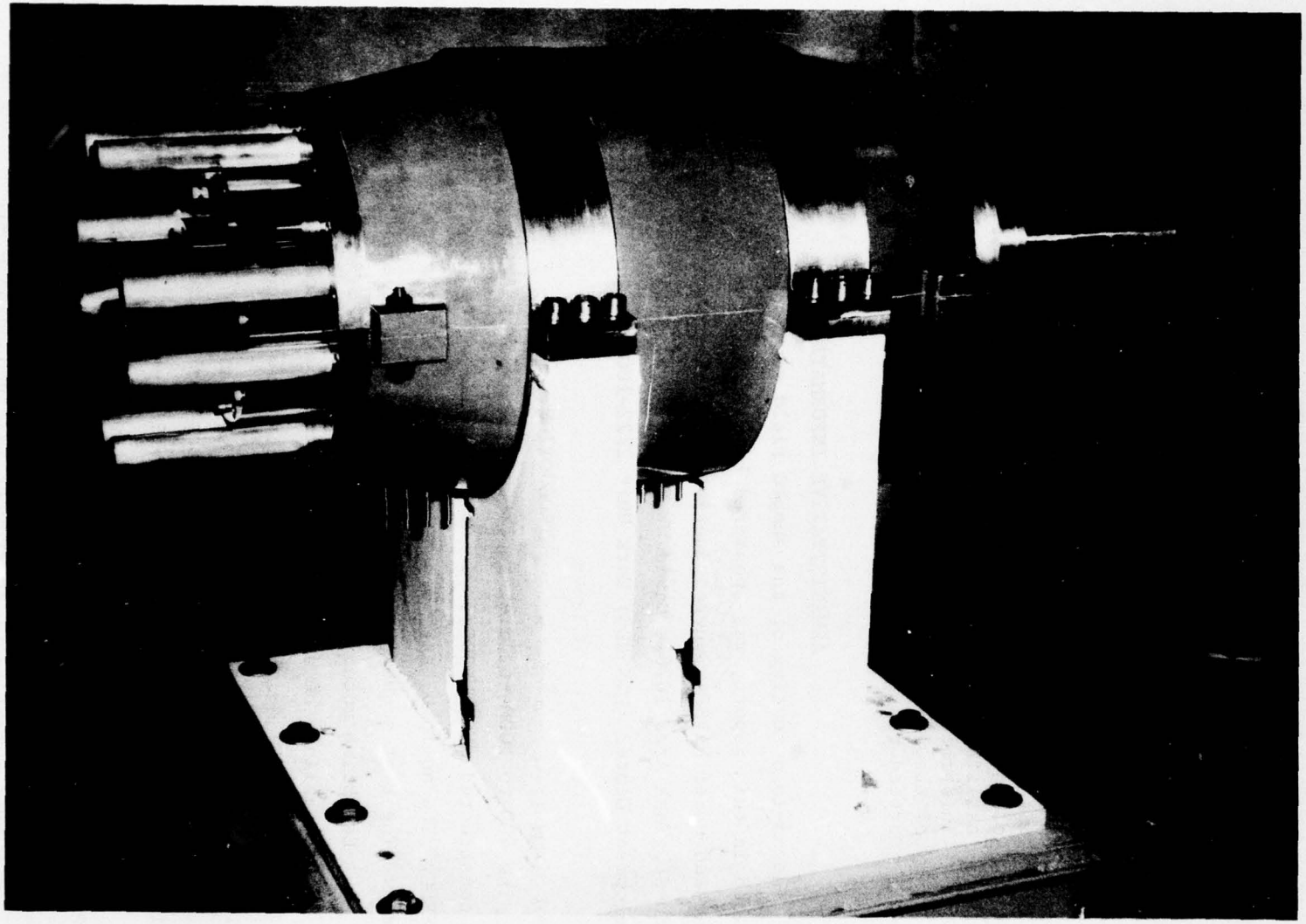

Figure 1 - Shaped Field Laboratory Motor

6. Establish operating procedures, instrumentation requirements, and techniques for handling liquid metal collector fluids and cryogenic helium.

This report is a documentation of the no-load testing which has been completed and a recommendation for modifications to the motor and for future test plans. The five main sections in the report are concerned with:

1. Machine Development: summary of the design and construction of the laboratory motor

2. Loss Analysis: review of the machine loss predictions

3. Test History: chronological discussions of testing; procedures, problems, solutions, results

4. Results: test data summarized in tables and graphs with comparison between measured and predicted machine loss data

5. Conclusions and Recommendations: summary of qualitative test results with discussion of modifications made during testing, suggestions for additional modifications, and a recommended load test program.

Future tests will include load testing using a 10,000 amp rectifier power supply and dynamometer. Later the rectifier will be replaced by a superconducting generator powered by an LM-100 gas turbine. Successful laboratory operation of the motor and generator as a system will be followed by shipboard testing aboard a small testbed vehicle. These will be the subject of future test and evaluation reports.

MACHINE DEVELOPMENT

Major design features of the shaped field laboratory machine are shown in Figures 2 and 3 in cross sectional and isometric views. The solenoidal superconducting magnet is enclosed in the double-walled, vacuum-insulated, helium dewar and is supported by the rotor at one end through an idler bearing. At the opposite end, the dewar neck, which contains the helium inlet and exhaust lines and power leads, is rigidly attached to one bearing housing. The winding includes 13,340 turns of 0.030-in. O.D. filamentary niobium titanium superconductor providing magnetomotive forces approaching 2 million-ampere turns.

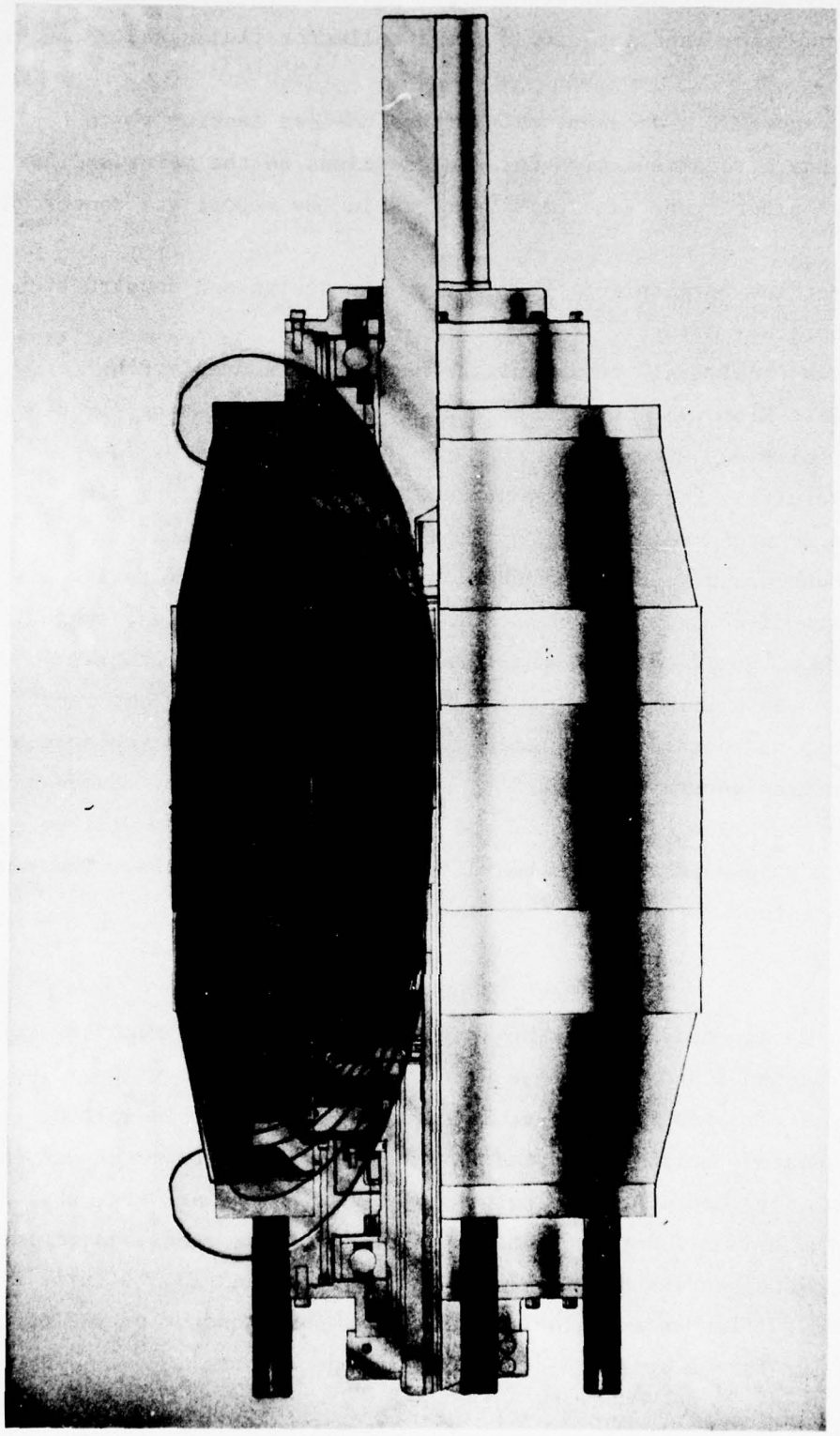

Figure 2 - Motor Cross Section with Flux Plot

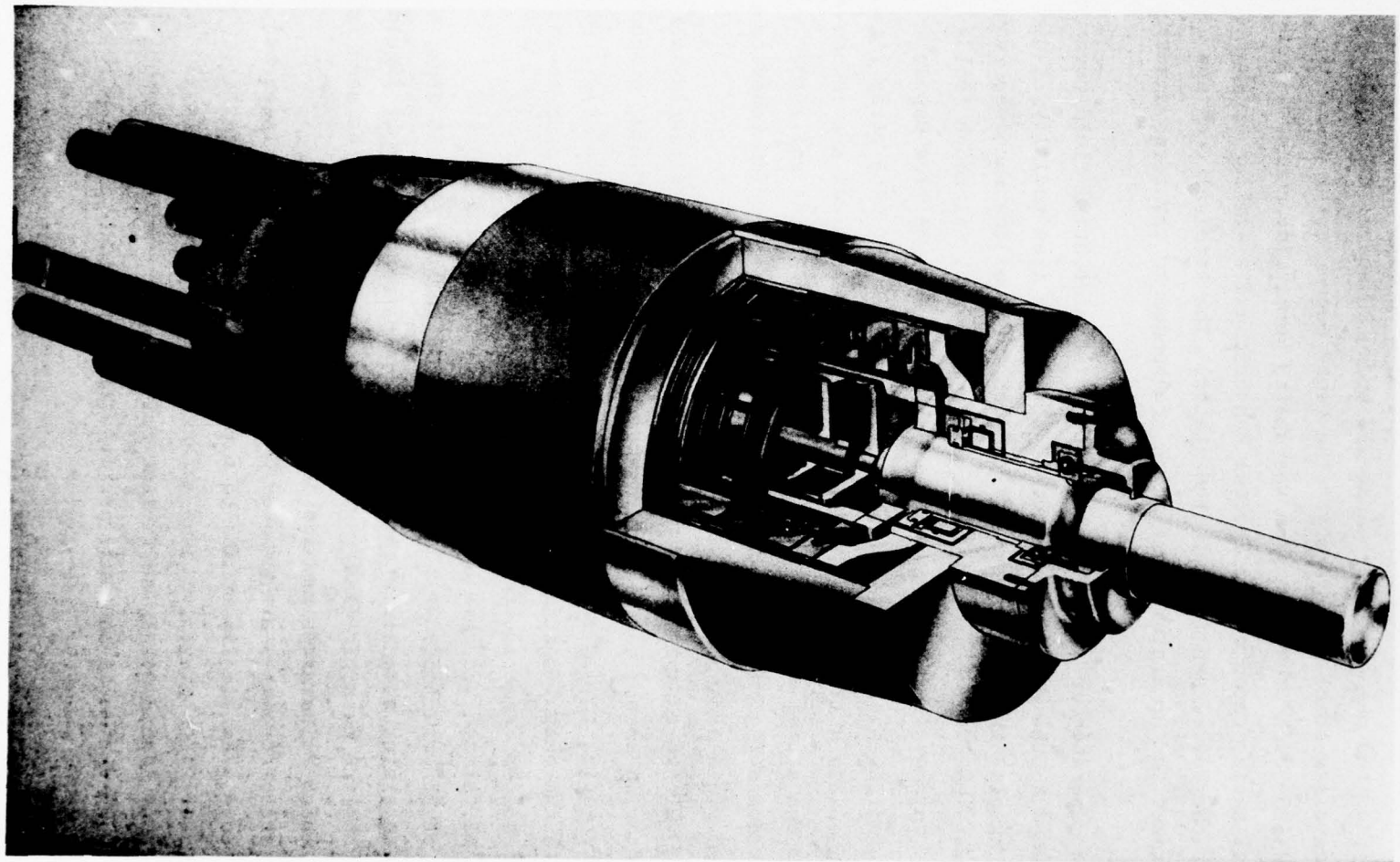

Figure 3 - Shaped Field Laboratory Motor Isometric

The in-line sets of four concentric drum conductors are symmetrically located about the magnet center plane and epoxy bonded to the outer surface of the stainless steel rotor shaft. The eight copper rotor drums are insulated from each other and from the shaft, permitting connection in electrical series through liquid-metal brushes, and a similar arrangement of copper current return drums in the stator. The terminal rods are silver brazed to the stator drums which are bonded to the ferromagnetic shield.

Flux generated in the solenoid by the circumferential field current is attracted to the steel shielding. Entering the iron radially, flux proceeds axially through the iron to the other end of the machine, returning radially to the magnet bore to complete the path. Although fields of 55,000 to 70,000 G exist in the magnet, the superimposed flux map in Figure 3 indicates extremely effective flux containment with stray fields outside the shield limited to less than 100 G. Field lines are concentrated in the active drum regions and widely spaced at the collector sites, illustrating the flux utilization and loss suppression benefits of the shaped field arrangement.

When voltage is applied at the terminal rods, the resultant axial current flow in each rotor drum interacts with the radial field, producing a circumferential torque. The cumulative torque developed in each drum is coupled to the output shafting through the drum-to-drum and drum-to-shaft insulated bonds. Reaction torque produced in the stator drums is transmitted through the shielding to the machine mounting points.

The brush work includes 16 copper rotor disks, two on each drum, each rotating in stator channels with the disk-channel gap bridged by liquid sodium-potassium eutectic (NaK). The collector geometry can be seen in Figure 4 which illustrates machine assembly.

The stator channels are grooves cut into copper stator rings; two annular rings electrically bonded to each stator drum. An unflooded operating mode is employed with no external NaK circulation. Small quantities of liquid metal, sufficient only to assure uniform contact around the disk-channel annulus, are injected into each channel with

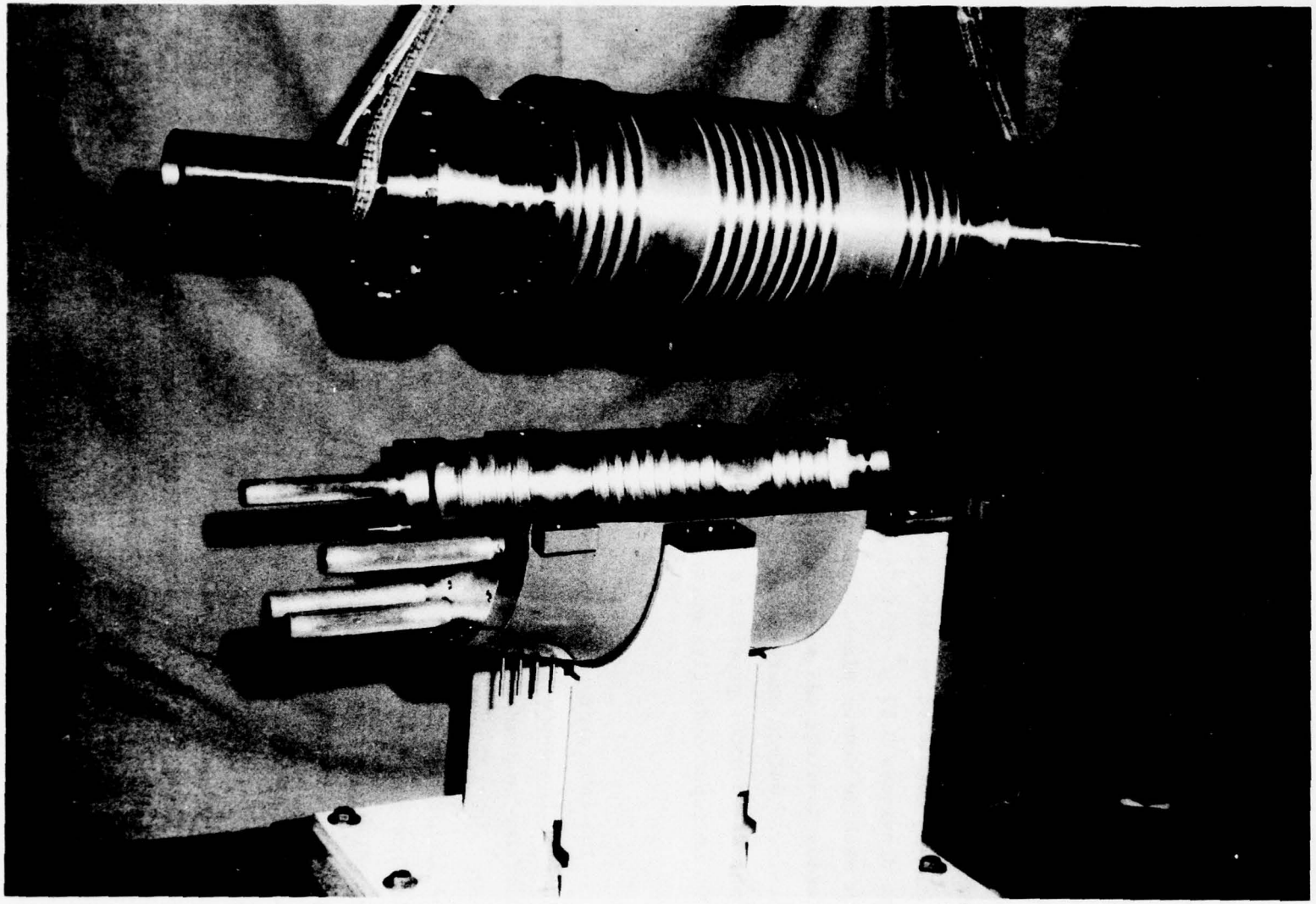

Figure 4 - Rotor Placement in Bottom Stator Half

centrifugal and magnetohydrodynamic forces providing NaK distribution. The fluid pools at the bottom of each channel during periods of non-operation. A dry, oxygen-free cover gas (such as argon) maintains long-term NaK purity.

A nonconducting coolant fluid is circulated through parallel tubes in the stator rings to remove resistance and viscous drag-generated heat. Most of the heat originating in the rotor is transferred by conduction to the stator rings across the liquid metal collectors, with a lesser portion radiated and convected to the stator drum assembly and the fluid-cooled dewar surface.

The completed machine, shown in Figure 5, weighs 1050 kg (2300 lb) and displaces 0.17 m^3 (6 ft^3), with a (maximum) 51 cm (20 in.) diameter at the machine center plane. The shield is 76 cm (30 in.) long and the bearing housings add an additional 10 cm (4 in.) at each end of the machine. Output shafting is 10 cm (4 in.) in diameter. The conventional 25-hp drive motor provides a dramatic size comparison with the 400 to 1000 hp superconductive unit.

LOSS ANALYSIS

The laboratory motor losses* can be divided into two categories. The first is the ohmic loss in the armature circuit which can be neglected under the no-load test conditions (except for short-circuit tests). This leaves viscous drag losses, the preponderance of which are associated with the liquid metal current collectors used in the motor. There exist three distinct loss mechanisms: bearings, seals, and windage; viscous drag in the collectors; and circulating current in the collector. The loss equations are based on the listed parameter values and on the collector geometry and liquid sodium-potassium (NaK) distribution illustrated in Figure 6.

The windage power loss, due to air in the magnet-rotor annular gap and the cover gas in the rotor-stator annulus, is predicted to be proportional to the square of the machine speed n.

---

*The motor losses were treated in detail by Cannell and Doyle and are summarized (and refined as appropriate) in this section.

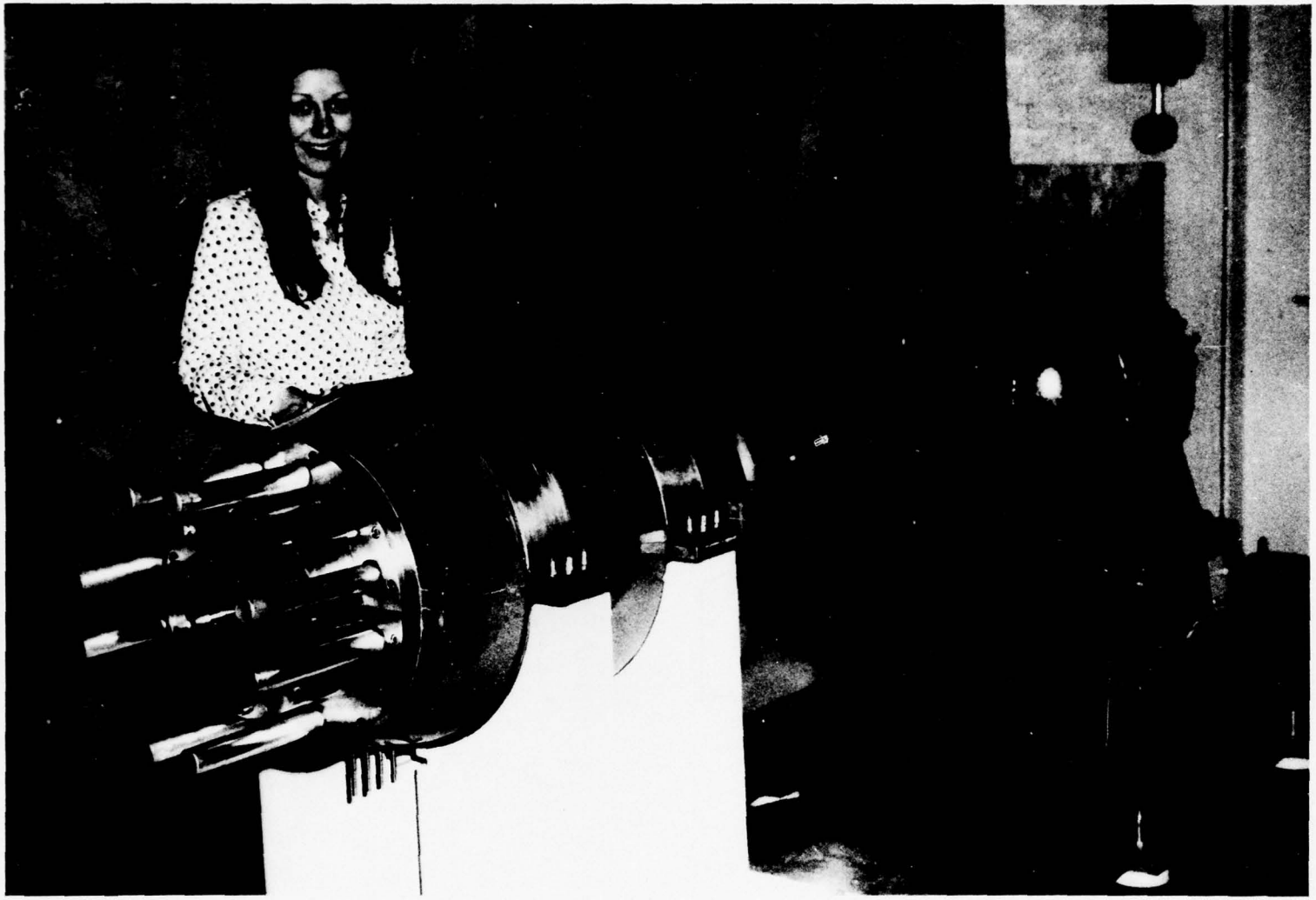

Figure 5 - Assembled Machine being Readied for No-Load Testing

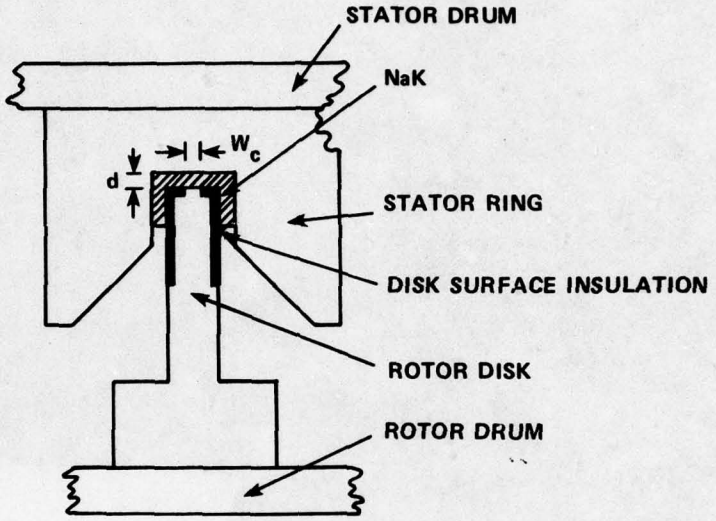

n = Machine speed (r/min)

I_f = Field current (amp)

B_{cr} = Radial field (tesla)

V_c = Average fluid velocity = $8.25\ (10^{-3})n\ (m/s^2)$

A_c = Collector area = $0.001935\ (m^2)$

A_{dw} = Disk wetted surface = $0.0058\ (m^2)$

d = Collector gap = 0.0005 (m)

W_c = Collector width (effective) = 0.00198 (m)

f = Fanning friction factor = 0.007

ρ_{NaK} = NaK density = $850\ (kg/m^3)$

σ_{NaK} = NaK resistivity = 45×10^{-6} (Ω-cm)

Figure 6 - Collector Geometry and Parameter Values

$$P_{cw} = (1.25 \times 10^{-5})\ n^2 \text{ watts} \quad (1)$$

The bearings and seals power loss due to friction is proportional to machine speed:

$$P_{cbs} \approx 0.29\ n \text{ watts} \quad (2)$$

Thus, the total "base" power loss (without liquid metal or field effects) can be expressed by the following equation:

$$P_{cwbs} = (1.25 \times 10^{-5})\ n^2 + 0.29\ n \text{ watts} \quad (3)$$

where the proportionality constants are derived estimates.

The expression for viscous drag loss due to the liquid metal appears as follows:

$$P_{cv} = 16f\ \rho_{NaK} V_c^3 A_{dw} = (3.1 \times 10^{-7})\ n^3 \text{ watts} \quad (4)$$

The viscous loss is proportional to the speed cubed since turbulent flow exists at all machine speeds above 300-500 r/min. The equation shows the sensitivity to changes in the disk wetted surface (A_{dw}) which result from changes in NaK volume. The viscous loss estimates for the motor are based on a wetted surface of 58 cm^2 and the assumed NaK distribution in Figure 6.

The third loss mechanism results from the interaction between the circulating current loops and the magnetic field present in the collector region. The radial field component creates an axial voltage gradient in the rotating collector disk which is shorted by the stator through the NaK, setting up the circulating current loops. The expression for the resulting loss term is:

$$P_{cc} = \frac{B_{cr}^2 \, W_c^2 \, V_c^2}{\sigma_{NaK}} \left(\frac{1}{3d} + \frac{d}{4(W_c + d)^2} \right) \cdot A_c \text{ watts} \qquad (5)$$

where the first term in parentheses is due to the radial component of the circulating current and contributes the bulk of the power loss. The second term accounts for the effect of the axial component, which is small compared to the radial field effects in the motor, and was neglected.

Using the field values generated by the TRIM magnetic analysis procedure developed at Argonne National Laboratory, the radial field component (B_{cr}) at each brush site can be expressed as a linear function of the field current (I_f).* Summing over the 16 brush sites, the total B_{cr}^2 term in Equation (5) can be expressed as:

$$B_{cr}^2 = (10.56 \times 10^{-5}) \, I_f^2 \text{ tesla}^2 \qquad (6)$$

The power loss equation thus reduces to:

$$P_{cc} = (8.324 \times 10^{-8}) \, n^2 \, I_f^2 \text{ watts} \qquad (7)$$

In deriving Equation (7), it was assumed that the current crosses the collector gap in straight line paths. Actually, the current fans out in the NaK and uses a larger conducting surface than just the uninsulated surface of the brush tip. A 25 percent margin is included in the effective collector area to account for this. Subsequent analyses confirm the accuracy of this margin.

An additional current-field interaction takes place in the collector region which generates negligible power loss, but produces forces on the NaK which could cause ejection of the fluid from the brush sites. The load current interacts with the circumferential field generated by the toroidal load current path through the machine and causes large axial body

*See Appendix A.

forces on the NaK. Normally the motor will operate at speeds which will produce a restoring centrifugal force sufficient to counteract the ejection and provide uniform NaK distribution. However, at low speed, high torque (high current) operations, such as sudden acceleration or reversal, ejection will be a serious problem with the present simple collector design.

Referring to Figure 7, it is possible to predict the range of machine operation in which ejection is likely to occur by calculating the ejection pressure (P_{ej}) and the restoring pressure (P_{res}). The speed-current combinations for which $P_{ej} > P_{res}$ will cause ejection. The load current (I_{ej}) at which the pressures are balanced is, thus, related to speed by the following expression:*

$$I_{ej} = 16.8\ n \text{ amps} \tag{8}$$

In the motor configuration, the terminal voltage is equal to the sum of the back electromotive force (V_{emf}) and the voltage drop across the machine resistance (V_{Ω}).

$$V_T = V_{emf} + V_{\Omega} = N\ \Phi_E\ n/60 + R_{\Omega} I_1 \tag{9}$$

where N = number of rotor drums = 8

n = rotor speed (r/min)

Φ_E = average effective radial flux = $0.803 \times 10^{-3}\ I_f$ (webers)

R_{Ω} = machine resistance = $30.3 \times 10^{-6}\ \Omega$

I_1 = load current (amp)

Under no-load test conditions (excluding the short-circuit tests) the load current is very small and the second term in the expression becomes negligible. Thus, the terminal voltage expression reduces to:

$$V_T = (1.08 \times 10^{-4})\ I_f n \text{ volts} \tag{10}$$

---

*See Appendix B.

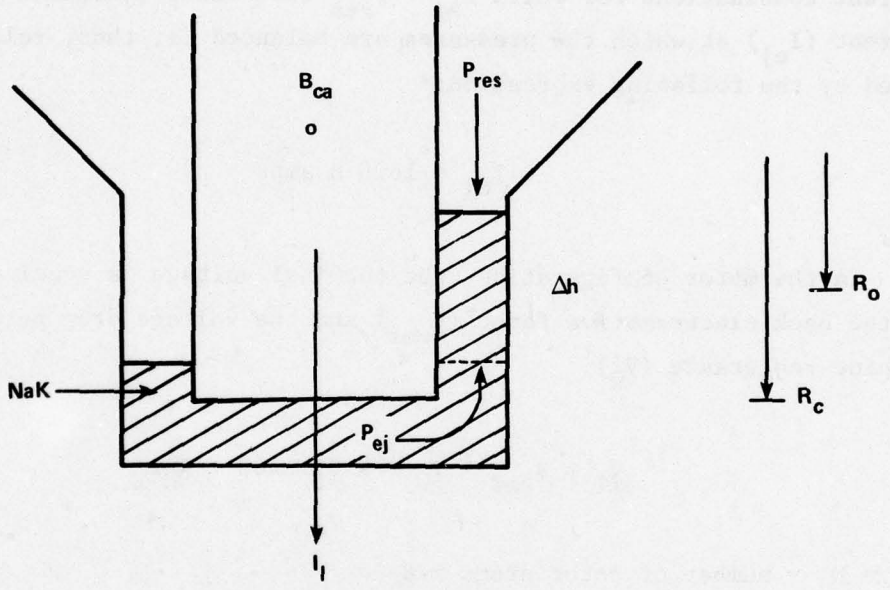

Figure 7 - Model for Ejection Calculations

TEST HISTORY

Machine no-load performance was evaluated with NaK inventories of 2, 3, 4, and 5 cc per brush site over a machine speed range of 300 to 1800 r/min and at field currents of 0 to 120 amp. Machine speed was measured using a toothed gear with a digital readout displayed on the instrument panel. Torque on the motor shaft was measured with a strain gage torque transducer and the digital readout was displayed on the instrument panel. Magnet field current was provided by a power supply capable of both constant current and constant ramp rate modes of operation. A voltage was applied across the coil terminals and the field current ramped up to the desired value at a selected ramp rate. (Ramp rates of 15 to 100 min to the rated value were available.) Voltage and current were displayed on the front panel of the power supply.

LIQUID METAL HANDLING PROCEDURE

The NaK fill procedure illustrated in Figure 8 was devised, was successful in making the test conditions repeatable, and, therefore, made the test data meaningful.

Initially, all valves are closed with all the NaK in the reservoir. The manifold is then evacuated to prevent gas pockets above the NaK in the fill tubes. Valve A is then opened allowing the NaK to flow into the calibrated sight glass. Then, valve A is closed, valve B is opened, and pressurized cover gas (argon) pushes the NaK out of the sight glass and into the manifold (Figure 9). Due to space limitations, the manifold is staggered to allow access to all brush sites. The NaK is then added to the brush sites one at a time by opening the respective valve (1, 2, ...) with the others closed. The fluid volume which enters each brush site is indicated by the drop in the level in the sight glass, however, there is a "dead-zone" between the manifold and the collectors so that not all of the NaK, which comes from the sight glass, actually gets into the collector channel. The fluid level in the sight glass must, therefore, be allowed to drop the desired amount plus the amount necessary to account for the

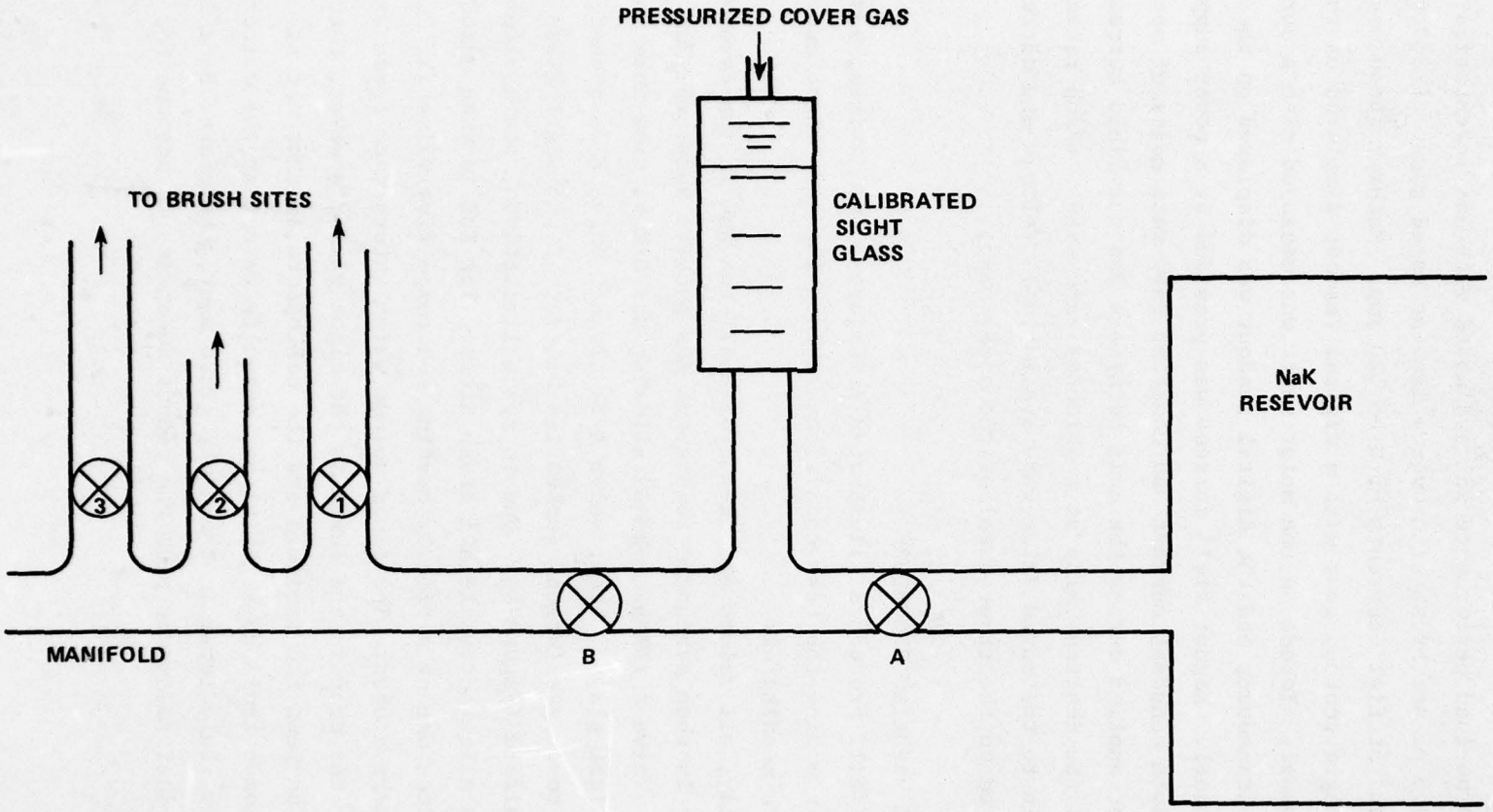

Figure 8 - NaK Fill System Schematic

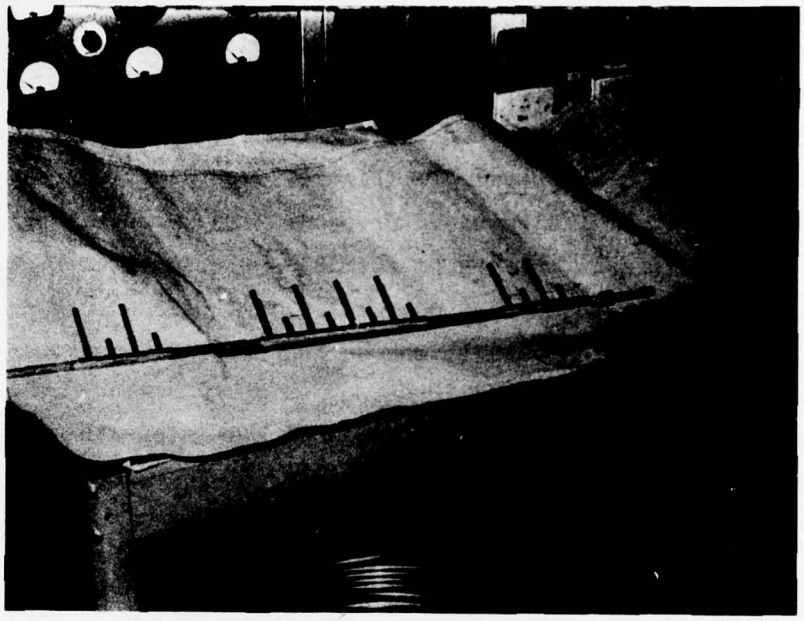

Figure 9 - NaK Fill Manifold

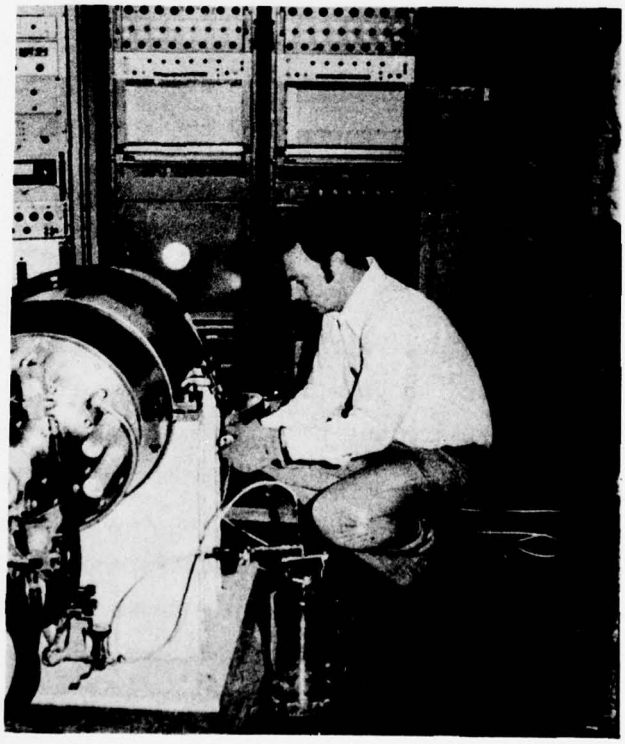

Figure 10 - NaK being Removed from System

dead-zone. Every other sight receives a little extra NaK to account for the staggering. The sight glass is replenished when necessary by repeating the first steps of the procedure.

Originally, the NaK was removed from the machine directly into a bottle half filled with mineral oil (Figure 10), then the system was purged with mineral oil followed by propanol. The propanol reacted with the residual NaK left in the system forming a precipitate which was removed with water or additional propanol. The residue left on the copper surface blackened when exposed to the atmosphere and was extremely difficult to remove.

It was subsequently decided to abandon in-machine cleanup procedures. As much NaK as possible was drained from the machine which was then opened. The remaining NaK was reacted with water and flushed from the machine.

Although this NaK fill setup made the test conditions repeatable, it was still impossible to determine exactly how much NaK was actually in the collector channel, and an improved procedure was sought.

Presently, NaK is inserted and removed from the collector sites through a rubber septum using a hypodermic needle and calibrated syringes. This method provides accurate control over the actual NaK volume placed in each collector site.

LIQUID HELIUM SUPPLY

The liquid helium used to cool the magnet coil to cryogenic temperatures was transferred directly to the magnet dewar from the supply dewar. Helium gas was used to provide a back pressure in the supply dewar which forced the liquid helium out through the transfer line and into the magnet dewar. As helium boils off during operation of the magnet, the gas is vented from the magnet dewar. By adjusting the venting, the pressure in the magnet dewar can be regulated. The difference between the pressures in the magnet dewar and the supply dewar determines the rate of helium flow. Approximately 70 L of liquid helium were required to initially cool down the magnet over a time span of 6 hr. This figure

became 150 L if the cool down time was reduced to 2 hr. During testing, the helium flow rate was approximately 10 L/hr.

TEST SEQUENCE

The machine was operated both as a motor and a generator using the testing setup shown in Figure 11. In the generator configuration, the machine was powered by a 25-hp drive motor with torque versus r/min measurements being recorded at various field currents. First the machine was run without NaK and at zero field to determine the bearings, seals, and windage losses. NaK was then introduced to the brush sites, with the field current still at zero amp, to determine the viscous drag loss, which was equal to the measured power loss minus the bearings, seals, and windage losses. The field current was then increased to measure the circulating current loss as a function of both field current and speed. The circulating current loss was equal to the total measured power loss minus the power loss at zero field current. In the motor configuration, the terminals were connected to a 1000 amp, d.c. power supply; voltage and speed data were recorded.*

To investigate the previously mentioned ejection problem, short circuit tests were conducted. The motor terminals were shorted (Figure 12) and the shaft was turned by the d.c. drive motor. The machine speed was set at a particular value and then the magnet current was increased until ejection of the NaK from the channel was observed. Under the no-load test conditions, it was not possible to examine low speed and high current operation. This range of operation will be investigated as a part of the load test program.

The first operation of the machine occurred in January 1973 when it was run in the motor configuration (Figure 13). The motor ran quietly without incident for several hours until the carbon seals wore out (wrong grade of carbon due to manufacturer's error). From this initial operation, several modifications were found to be desirable. While waiting for replacement seals, these modifications were instituted in the machine. The main machine bearings were changed to the shielded ball

---

*Test data will be presented in the "Results" section.

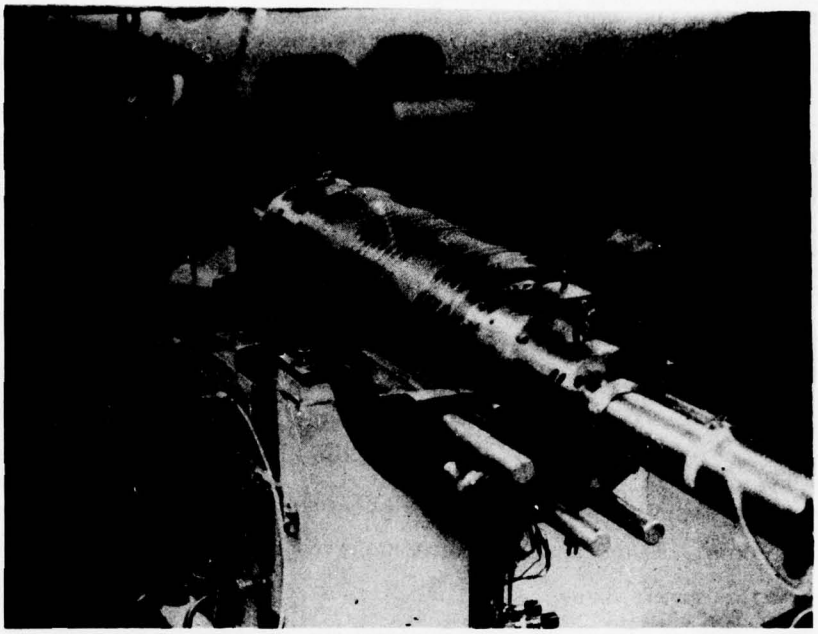

Figure 11 - Machine being Assembled in No-Load Test Configuration

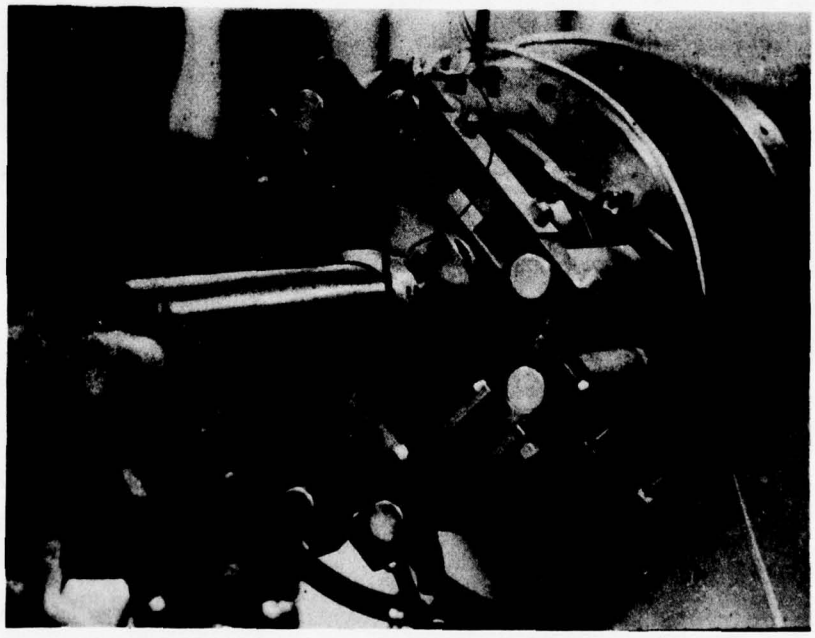

Figure 12 - Short Circuited Motor Terminals

bearing type enclosed in a water jacket. Several changes were made in the magnet dewar system. The dewar pilot bearing was replaced with a sealed ball bearing. The dewar itself was enclosed in a water jacket (Figure 14) to reduce helium boiloff caused by a rise in temperature as the rotor heats up during operation. Finally, the dewar neck was redesigned to accommodate conventional helium transfer lines which have higher heat leakage but are much easier to handle than the large, low loss lines supplied with the magnet system (Figure 15). The new dewar neck design permitted the machine to be disassembled and assembled without warming up the magnet which was not possible with the original helium supply system. The confusion of leads shown in Figure 16 was eliminated providing a quicker and easier electrical hookup for instrumentation. The new design made a substantial reduction in the time and effort required to assemble and disassemble the machine.

These modifications were completed and no-load testing was resumed October 24, 1973. The machine was operated in the generator configuration using the test rig (Figure 17) to check out the modifications and to establish operating and data recording procedures. On November 6, 1973, generator configuration tests at a NaK inventory of 2 cc per site were conducted. Data were recorded for field currents of 0, 25, 50, and 75 amp, but the 50 and 75 amp data indicated an increasing loss of conductivity in the collectors due to contamination of the NaK with coolant. After disassembly, it appeared that thermal expansion in the machine caused cracks in the epoxy joints. Coolanol leaked through these cracks and contaminated the NaK. To absolutely prevent further leakage, anodized aluminum tubing was inserted into the cooling holes drilled in the stator ring; this allowed water, with much improved fluid characteristics, to be substituted for the coolanol.

On December 12, 1973, test data were taken over the entire test operating range. This made it possible to analyze the loss data for the first time. The bearings, seals, and windage losses were slightly lower than estimated, while the viscous drag loss agreed closely with the

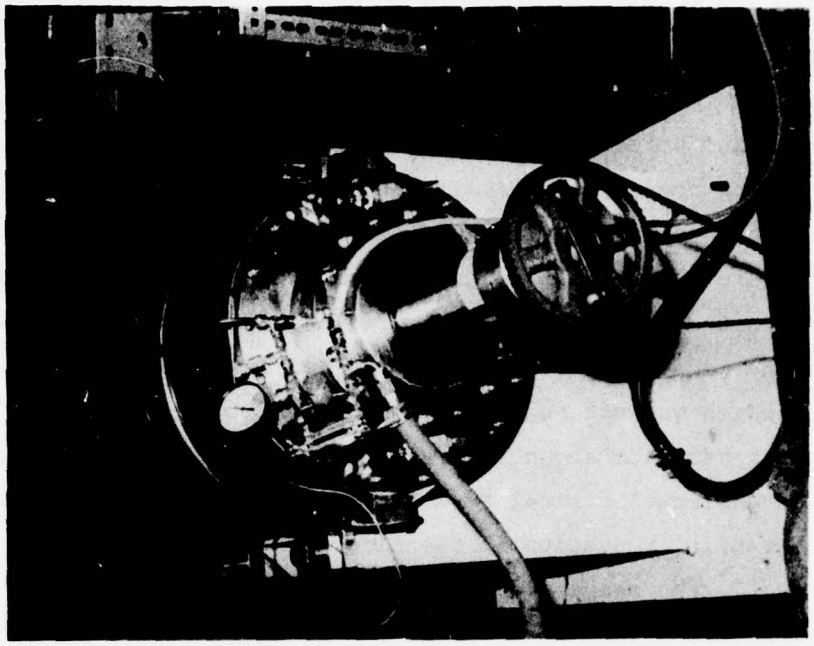

Figure 13 - Machine in Motor Configuration during Initial Testing

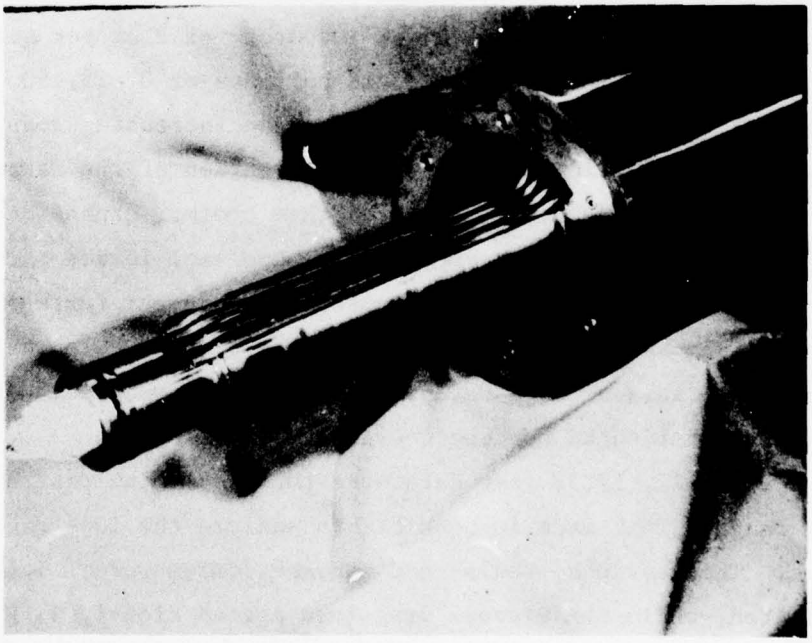

Figure 14 - Magnet Dewar with Water Jacket

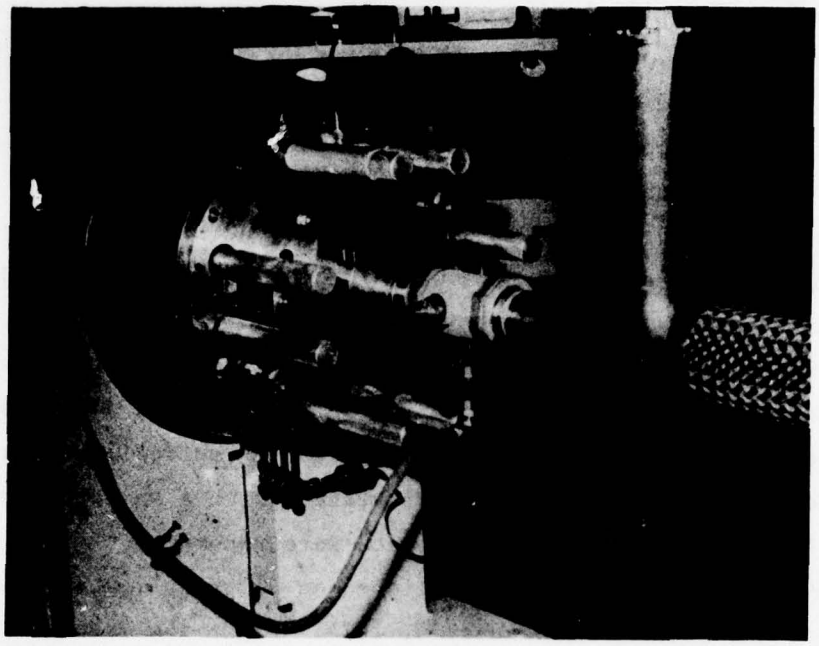

Figure 15 - Original Helium Transfer Line

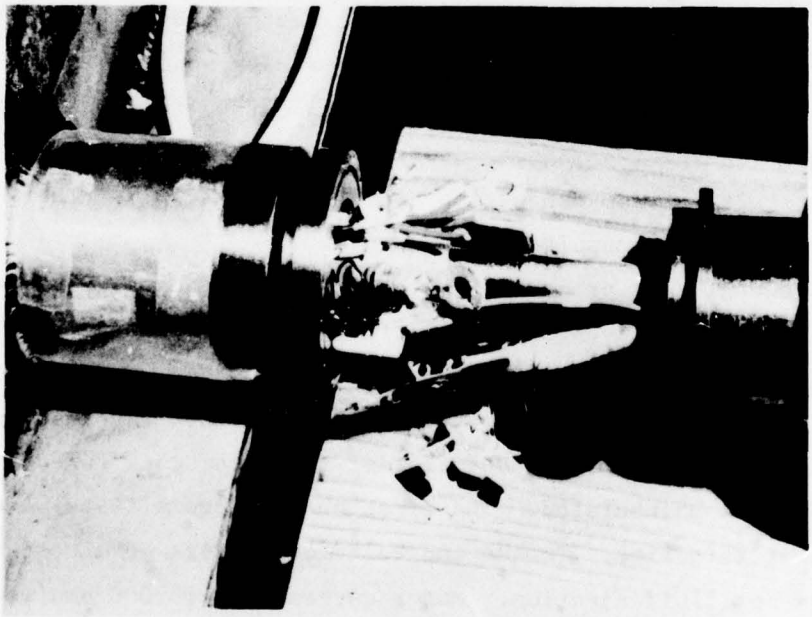

Figure 16 - Original Dewar Neck Showing Confusion of Leads

predictions. The circulating current loss was much greater than calculated, as expected, because the brush tips were not yet insulated.

The zero field current test (at 2 cc NaK) to determine viscous drag loss was repeated on January 4, 1974, to corroborate the earlier testing, however, the resulting losses were lower than before. The NaK inventory was then increased to 3 cc NaK per site, and the test procedure was repeated. The viscous drag loss was higher for the increased NaK volume which was expected.

A test was conducted on January 14, 1974, to check the bearings, seals, and windage losses, but during the testing, the dewar water jacket developed a leak. The problem was corrected by soldering the water jacket to the dewar end flanges in place of sealing with a silicon rubber adhesive (RTV). Due to the leak, no useful data were recorded.

The experimental procedure followed on February 7, 1974, was similar to that of the testing on January 4, 1974. First the machine was operated at zero field without liquid-metal to determine the base losses. Viscous drag and circulating current loss data were recorded for a NaK inventory of 2 cc per site but these results were questionable due to erratic continuity across the collector gap indicated by the voltage readings. The NaK was replaced, this time at 3 cc per site, and the test procedure was repeated. Good continuity was obtained during this run, however, there was an unexpected magnet "quench" which occurred at 1500 r/min and 120 amp, resulting from exhaustion of the helium supply. There was no apparent damage as a result of the quench.

The general test procedure which had now been established was repeated with a NaK inventory of 4 cc per site on February 14, 1974. The viscous drag loss was greater than the loss for 3 cc per site which was expected due to the increased wetted surface. There was also an increase in circulating current loss over that of the 3 cc test, however, the brush tips were still uninsulated. The first short circuit tests were also conducted at this time. Torque and voltage readings were used as indicators for fluid ejection. Motor currents of 19,000 amp were obtained at machine speeds of 1000 and 1500 r/min and 8700 amp at 500 r/min. When

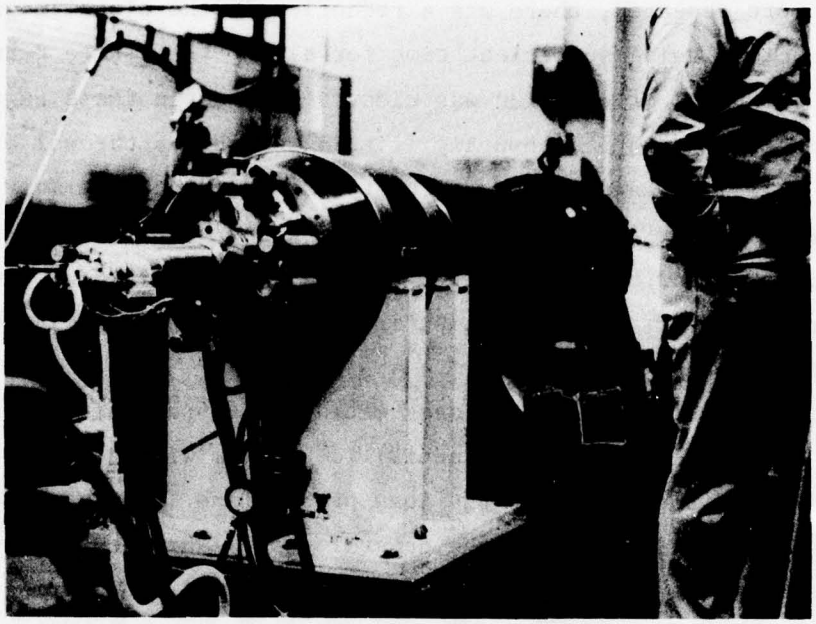

Figure 17 - Machine in Generator Configuration

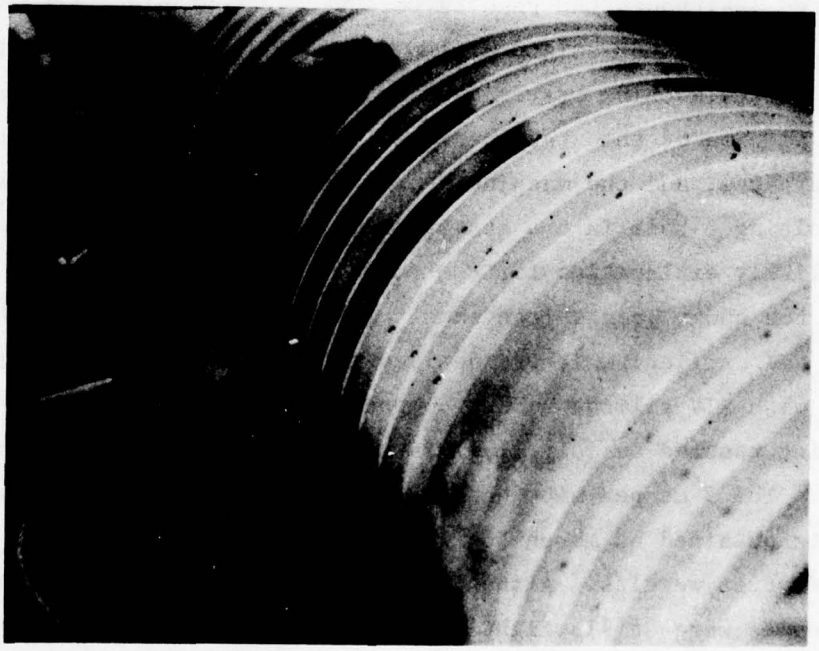

Figure 18 - Insulation being Applied to Collector Disks

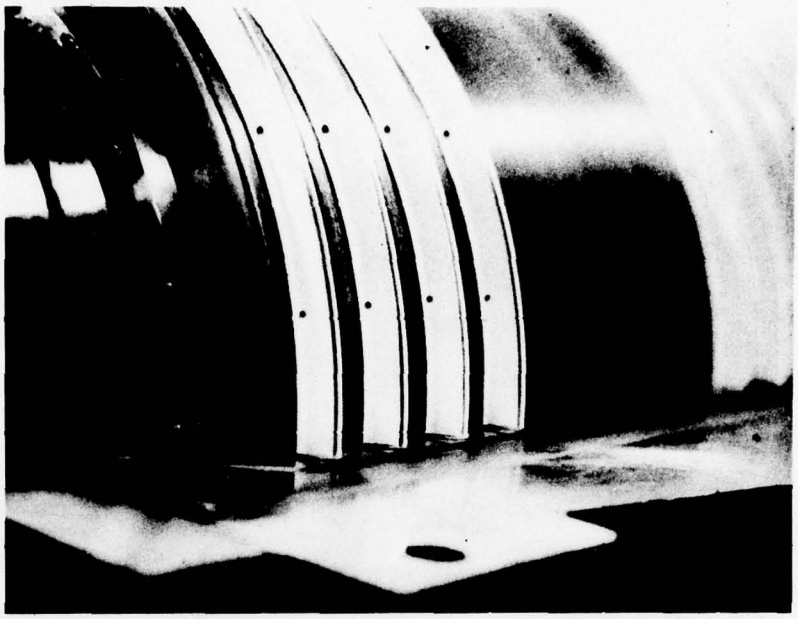

Figure 19 - Partially Insulated Collector Disks

Figure 20 - Hole in Stator Drum in Relation to Stator

Figure 21 - Closeup of Hole in Stator Drum

4 cc NaK per site tests were conducted. The viscous drag loss increased as expected, but the circulating current loss was slightly greater than expected. Speculation as to the reason for this unexpected result raised two possible answers. The original predictions might be deficient because of the assumption of an average magnetic field (B) in all 16 brush sites and/or there could have been circulating current loops within the NaK itself. At this time, the circulating current loss predictions were refined to the extent that they appear in this report. The latter possibility was the subject of later testing with fully insulated brush sites.

Results from the motor configuration test indicated that the average effective radial flux was lower than predicted.

Additional short-circuit testing also took place at this time. Currents of 20,000 to 30,000 amp were achieved at machine speeds of 1200 to 1800 r/min. Unlike the previous short-circuit tests, the NaK ejection was not clearly evident. There was only an instability of NaK continuity rather than a complete loss of continuity as evidenced in earlier testing. There was no sudden loss of current nor increase in speed; only an erratic current reading on the oscilloscope indicated ejection. The two most likely explanations for the differing results were: the partial insulation of the brushes and the existence of a uniformly continuous NaK distribution in the collectors. These results were very encouraging, relieving doubts raised by earlier short-circuit testing as to how much horsepower the motor was capable of producing under load. However, operation at low speed and high currents still remain a problem requiring further attention.

The last of the no-load testing to date (August 16, 1974) was conducted with fully insulated brush sites. Results of previous tests indicated that some of the collector loss was due to interaction between the field and the NaK independent of the brush conducting surface. By fully insulating the brush tips, the circulating current paths between the rotor disk tip and the stator ring were severed. Thus, the measured loss would be due to bearings, seals, and windage; viscous drag; and the NaK-field interaction loss. Tests were conducted with NaK inventories of 4 cc

and 5 cc per site. The data showed that a substantial percentage (40 percent) of the collector loss was due to circulating current loops within the NaK itself. There was little increase in loss when the NaK volume was increased, indicating that the preponderance of the field induced losses occurred near the brush tip.

RESULTS

The significant no-load test data are summarized in Tables 1 through 3 and Figures 22 through 25. The bearings, seals, and windage losses are mean values averaged over all the recorded test data. The collector viscous drag loss data are presented for 2, 3, and 4 cc of NaK per site, since sufficient data are available for these volumes to make averaging meaningful. Specific test case data are used to compare the predicted loss for both circulating current and total power. The negligible viscous drag and circulating current losses at 300 r/min are due to the change in the NaK velocity profile below 500 r/min when laminar flow is indicated as previously mentioned.

The data in Table 1 shows that the measured bearings, seals, and windage losses are substantially lower than predicted. The loss is approximately proportional to machine speed though with a smaller constant than originally guessed. At 1800 r/min the bearings, seals, and windage losses are approximately 0.5 kW, a small precentage of the total power loss.

The viscous drag loss predictions are based on a disk wetted surface of 58 cm, which corresponds to between 2.5 cc and 3 cc of NaK per site. The 3 cc data, therefore, agree more closely with the estimated loss. Figure 22 shows the 2 cc data are lower and the 4 cc data are higher than expected. All of the viscous drag losses are proportional to the cube of machine speed as predicted. At 1800 r/min the viscous drag loss is about 2 kW, assuming 3 cc of NaK per site.

The measured circulating current loss is well within 20 percent of the estimates over most of the operating range. Figure 23 shows the best accuracy occurs at higher field currents, where the measured losses are well within 10 percent and at some points within 5 percent of the predicted

TABLE 1 - BEARINGS, SEALS, AND WINDAGE LOSS

Machine Speed (r/min)	Power Loss (watts)	
	Test Data	Predicted
300	57	88
600	124	179
900	181	271
1200	247	366
1500	352	463
1800	496	563

TABLE 2 - COMPARISON OF CIRCULATING CURRENT LOSS FOR VARIOUS DEGREES OF INSULATION

Field Current (amp)	Machine Speed (r/min)	Power Loss (watts)		
		Uninsulated (February 14, 1974)	Partially Insulated (July 11, 1974)	Fully Insulated (August 16, 1974)
30	300	92	6	--
	600	369	28	14
	900	1289	80	53
	1200	1648	177	99
	1500	2930	275	195
	1800	4155	393	297
60	300	149	29	--
	600	838	138	57
	900	2077	324	138
	1200	3693	588	269
	1500	5912	921	425
	1800	7947	1168	616
90	300	138	55	4
	600	710	267	92
	900	2045	643	223
	1200	4091	1190	453
	1500	6942	1903	726
	1800	9843	2432	1104
120	300	--	97	11
	600	--	450	120
	900	--	1057	319
	1200	--	1940	623
	1500	--	3045	1044
	1800	--	4100	1593

TABLE 3 - TERMINAL VOLTAGE

Field Current (amp)	Machine Speed (r/min)	Load Current (amp)	Terminal Voltage	
			Test Data	Predicted
30	350	85	1.01	1.14
	660	175	1.98	2.14
	1360	450	4.00	4.42
	1905	775	5.58	6.20
60	1010	200	5.99	6.55
	2050	560	12.00	13.30
	2400	625	13.90	15.57
	2390	625	13.94	15.51
90	660	125	6.00	6.42
	1360	280	12.06	13.23
	2040	470	18.01	19.84
	2400	600	21.15	23.35
120	523	90	6.01	6.78
	1020	210	12.04	13.23
	1522	340	18.00	19.74
	2040	480	24.00	26.45
	2560	625	30.01	33.20
	1800	425	21.21	23.34

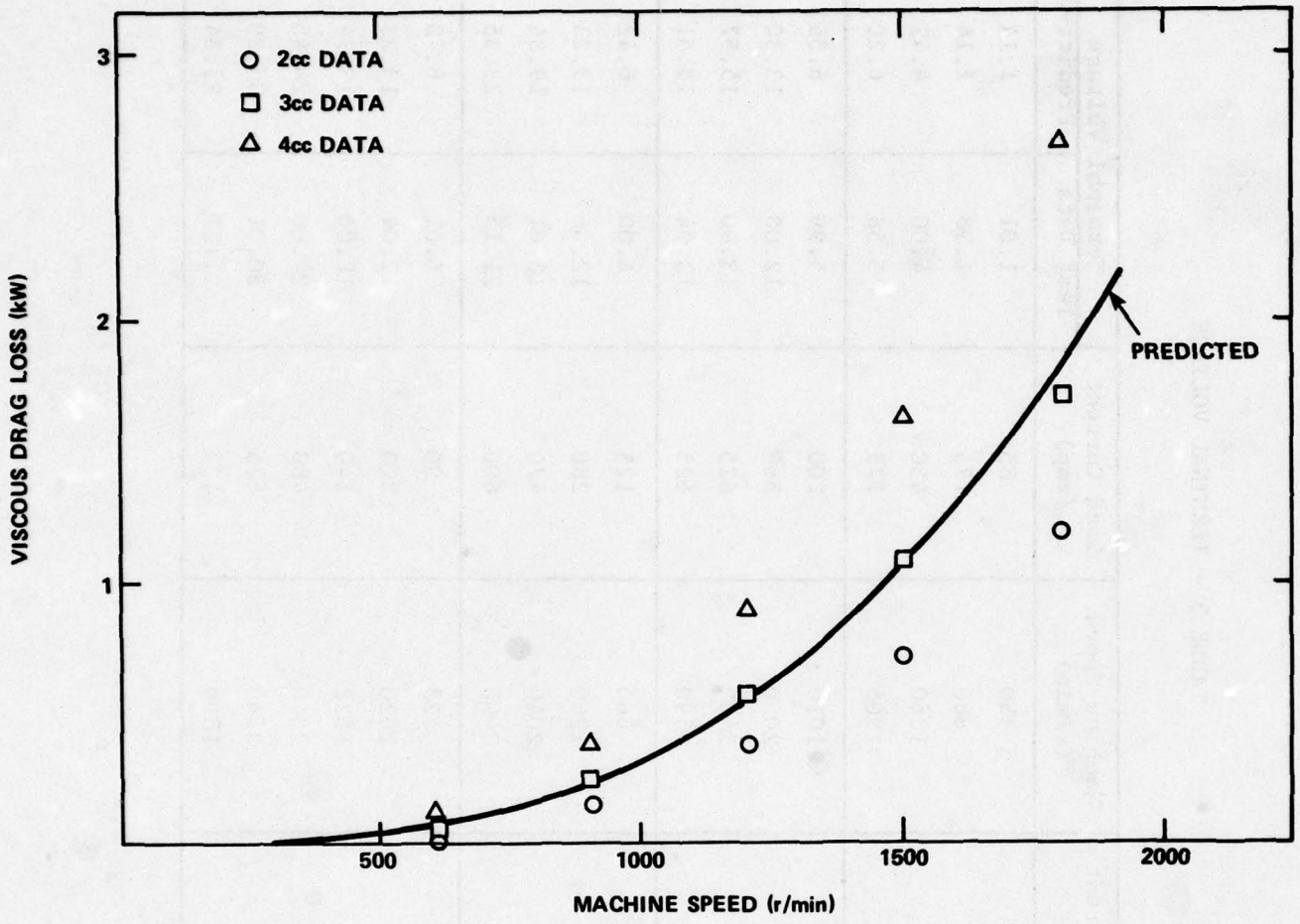

Figure 22 - Collector Viscous Drag Loss Characteristics

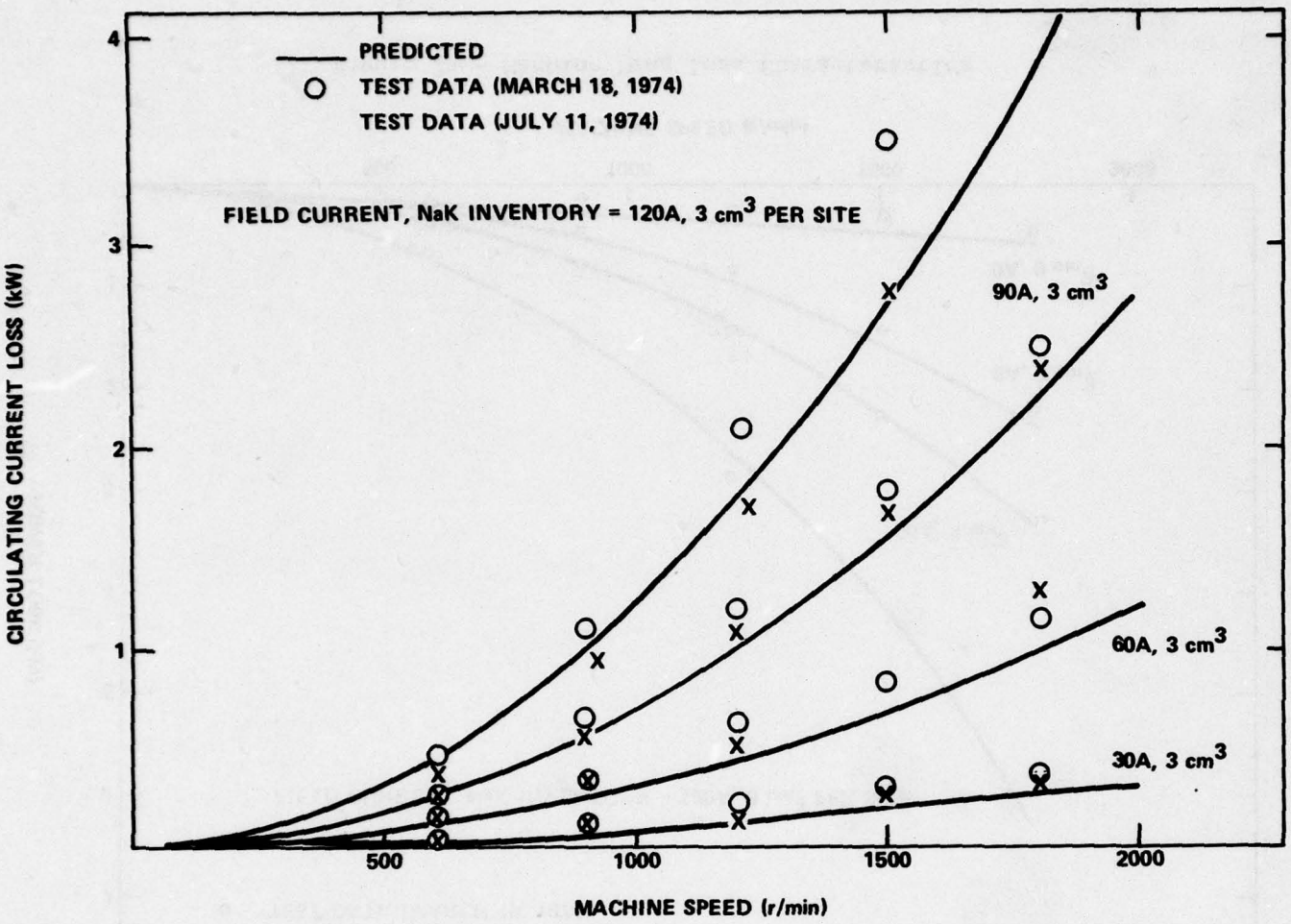

Figure 23 - Collector Circulating Current Loss Characteristics

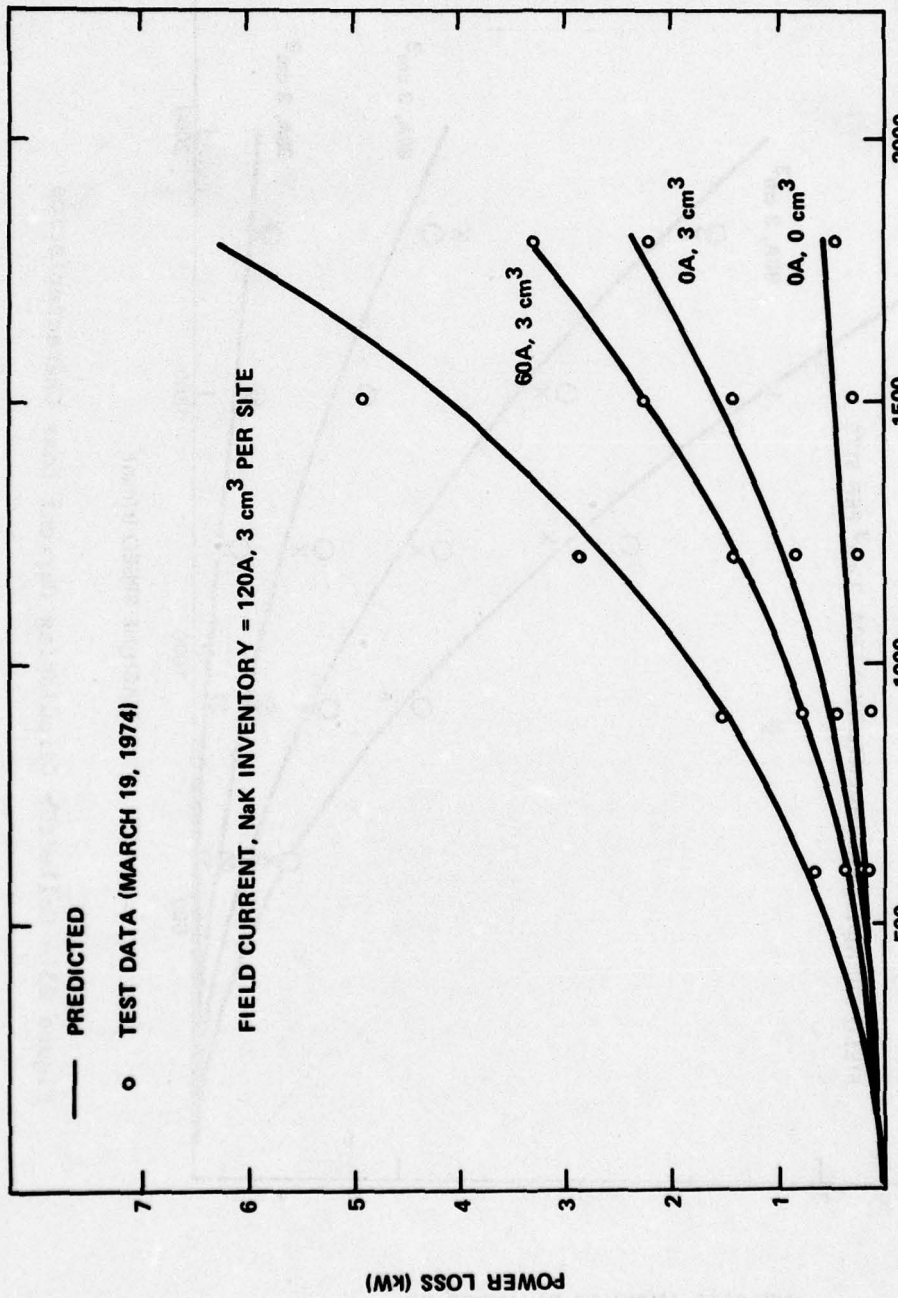

Figure 24 - Machine Drag Loss Characteristics

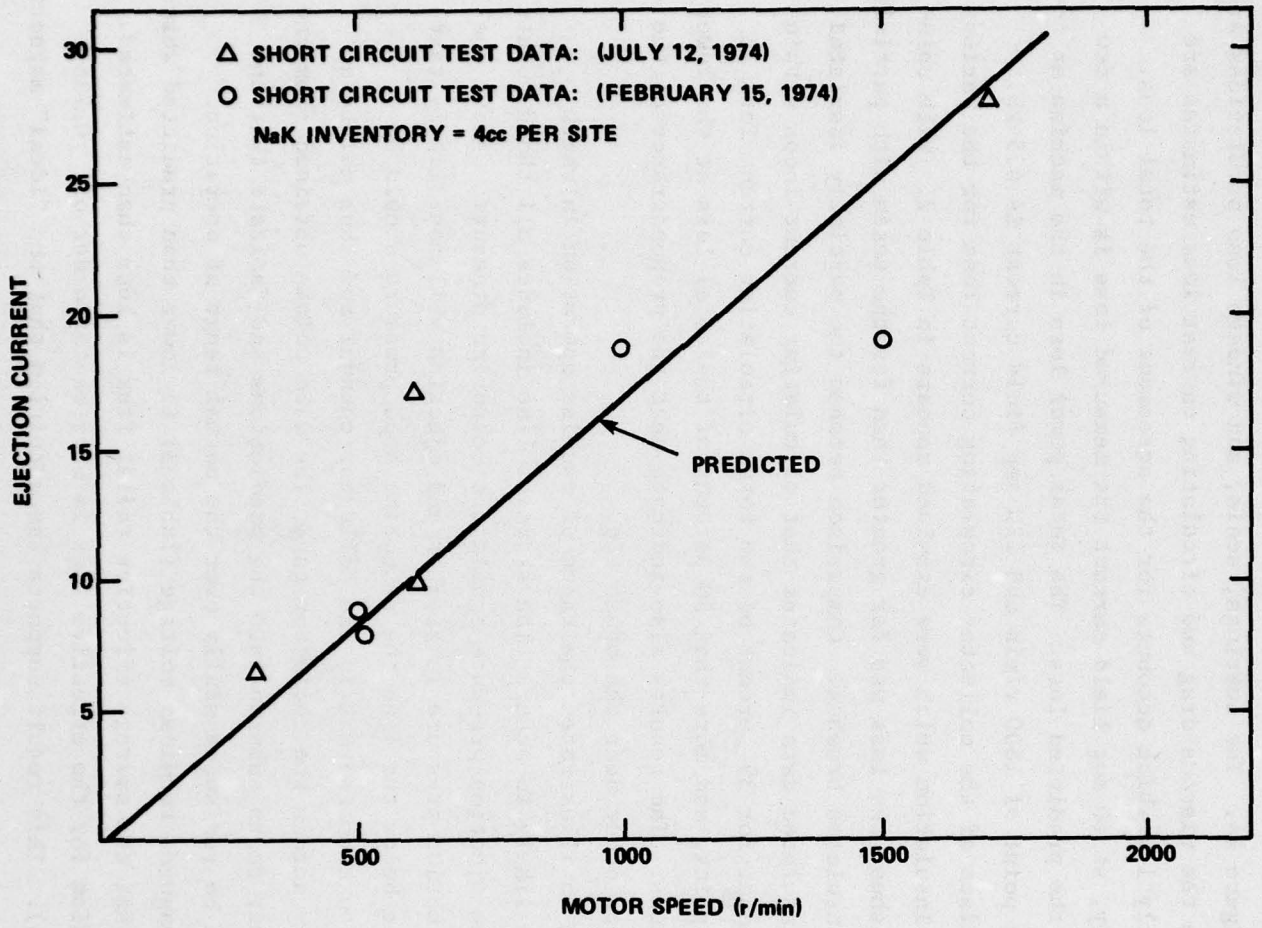

Figure 25 - Ejection Current versus Motor Speed

values. The predictions are poorest at lower speeds and field currents. At the 1800 r/min and 120 amp field current design point, the circulating current loss is 4 kW.

The total power loss measured agrees closely with the predictions as shown in Figure 24. The bearings, seals, and windage loss predictions are high, while the viscous drag and circulating current loss estimates are both slightly low which accounts for the agreement of the total loss. Specifically, at 60 amp field current the measured loss is within a few percent of the predicted loss. The total power loss in the machine at no-load design point of 1800 r/min and 120 amp field current is 6.5 kW.

Comparison of the collector circulating current loss for the various degrees of insulation which were examined appears in Table 2. With uninsulated brushes, the loss was far greater than for the tests with partially and fully insulated brushes. Comparison between the partially insulated and fully insulated data indicates that circulating current loops within the NaK account for 39 percent of the total circulating current loss at the design point, and more than 50 percent of the total loss at the lower field currents. The results also indicate that the preponderance of the current loops occur near the brush tip.

Figure 25 illustrates the range of machine operation in which ejection is likely to occur. The straight line includes all those points at which the ejection pressure equals the restoring pressure. Above the line the ejection pressure is greater and ejection will most likely take place, while below the line the restoring head pressure should be sufficient to keep the NaK in the collector channel and thus maintain conductivity across the collector gap. The data points obtained from the short circuit tests substantiate the predictions and indicate that the machine can be run successfully over the normal range of operation.

The measured terminal voltage (Table 3) is lower than predicted which indicates that the average effective radial flux is less than estimated. The expression for the effective flux is more on the order of: $0.735 \times 10^{-3} I_f$ (Wb). This result supports the suspicion that the "ideal" magnetic

properties of 1010 steel assumed were not reproduced in the motor shielding, since all of the required heat treatments necessary to optimize magnetic characteristics were not used in motor fabrication.

CONCLUSIONS AND RECOMMENDATIONS

The no-load test data substantially confirm the loss estimates although the loss equations are not completely accurate over the entire operating range. The bearings, seals, and windage losses are proportional to the square of the speed as was expected. The viscous drag loss is proportional to the cube of machine speed and the test data clearly show the dependence of the loss on NaK volume. The circulating current data indicate that the loss is a function of both the field current squared and machine speed squared. A comparison of the uninsulated versus partially insulated test data clearly shows the sensitivity of power loss to collector area (conducting portion of brush tip). The totally insulated test results show a substantial circulating current occurs within the NaK itself. These results indicate that the equations used for predicting motor losses can provide reasonably accurate estimates of the maximum losses expected at the design operating point for similar machines.

Results of the short circuit testing indicate that the motor can handle currents up to 30,000 amp at 1800 r/min necessary for operation with the 1000 hp turbogenerator. However, uncertainties about NaK ejection at low speed, high torque (high current) operation cannot be fully explored until load tests are begun.

Several modifications, made to the motor during no-load testing, could be recommended for future machine design. First, using RTV silicon rubber adhesive in place of epoxy for insulation between brush sites could eliminate cracking due to thermal expansion in the machine. Also, inserting anodized aluminum tubing into the cooling holes drilled in the stator rings prevents leakage of the coolant into the NaK channels.

The improved NaK injection system, using a hypodermic needle, provides accurate control over the actual volume of NaK placed in each site.

To reduce helium boiloff due to the rotor heating up during operation, the magnet dewar is enclosed in a water jacket. The redesigned dewar neck permits the use of conventional helium transfer lines which provide convenient operation and handling. Finally, sealed ball bearings are now used for the main machine bearings and the dewar pilot bearing.

Additional modifications, not presently instituted in the machine, seem worthy of consideration. The occurrence of shorts between drums during assembly and testing suggests the use of interfitting bars in place of the continuous drums. This would provide better spacing and would allow potting in the epoxy to virtually eliminate shorts. An improved cleanup procedure for flushing the NaK from the machine without disassembly would provide a "closed" liquid metal handling system eliminating exposure of personnel to the NaK. Such a system would be ideal for use aboard ship.

The no-load test results also established areas which required further study. The area of major concern is the NaK ejection problem. Although short circuit currents of 30,000 amp at 1800 r/min were obtained, the ejection problem at high torque (high current) and low speeds still remains. Analysis of the problem may lead to new collector designs which prevent ejection and reduce collector losses.* The other area which warrants study is machine losses under load conditions. Besides the ohmic loss which is a function of load current, there are interactions between the load current and the loss mechanisms investigated in no-load testing. Better insight into these interactions will result in more accurate estimates of the load performance. Such a study will also help in establishing the load plan by identifying the test conditions which will produce the most beneficial information.

The next step in the laboratory testing of the motor will be to conduct load tests using what has been learned from the no-load tests. Initially, it is necessary to check the instrumentation and operation of the test equipment; namely, the power supply and the motor connections. It is, therefore, advisable to run the motor without load at first to finalize the setup, and to familiarize test personnel with the experimental

---

*Alternative collector designs are being investigated under contract at this time.

procedures. After this check has been successfully completed, the output shaft would be connected to the dynamometer and the motor would be turned over and run under minimal loading and field current conditions. As confidence is gained, load and field can be increased to investigate motor performance over the entire operating range. Special care should be taken when operating under combinations of speed and load current which could cause ejection. Such combinations should be the subject of a separate test procedure which would determine the limits of operation for the motor in its present design.

Results of the load testing will be analyzed and compared to the predicted performance as reported by Cannell and Doyle.[1]

ACKNOWLEDGMENTS

The authors wish to acknowledge the many people whose efforts provided the information contained in this report. Design, construction, and performance predictions were provided by Mr. T.J. Doyle. Mr. Doyle also developed test requirements and plans. Mr. H.O. Stevens directed the setup and conduction of the tests with support from Messrs. H.H. Ferrero, J.C. Humphrey, L. Martin, F.E. McDonald, M.J. Superczynski, and H. Surosky. Mr. J. Stevens, Mr. H.O. Stevens, and Mr. M.J. Superczynski were responsible for machine modifications made during no-load operations with construction support from Mr. W. Umlandt, Mr. P. Owens, and Mr. H. Surosky, and analytical support from Mr. Doyle and Mr. G.F. Green. These efforts were produced under the direction and leadership of Dr. W.J. Levedahl and Mr. J.H. Harrison.

APPENDIX A

LINEAR RELATION BETWEEN RADIAL FIELD AND FIELD CURRENT

Below are the actual radial field (B_{cr}) values at eight of the brush sites (the values at the other eight are identical due to symmetry) as calculated by TRIM for field currents (I_f) of 100 and 125 amps.

Brush Site	B_{cr} at 100 amp (tesla)	B_{cr} at 125 amp (tesla)	K_i
1	0.047	0.059	0.47×10^{-3}
2	0.14	0.175	1.4×10^{-3}
3	0.241	0.300	2.4×10^{-3}
4	0.348	0.435	3.48×10^{-3}
5	0.388	0.485	3.88×10^{-3}
6	0.304	0.379	3.04×10^{-3}
7	0.232	0.289	2.32×10^{-3}
8	0.175	0.218	1.75×10^{-3}

The field at each site can be determined from the equation:

$$B_{cr}(i) = K_i I_f \text{ tesla} \tag{A.1}$$

where K_i is the constant of proportionality between B_{cr} and I_f. The total B_{cr}^2 used in the equation for circulating current losses is determined by summing the squares of the field at each site:

$$B_{cr}^2 = \sum_{i=1}^{16} B_{cr}^2(i) = 2 \sum_{i=1}^{8} B_{cr}^2(i) = 2I_f^2 \sum_{i=1}^{8} K_i \tag{A.2}$$

$$B_{cr}^2 = 10.56 \times 10^{-5} I_f^2 \text{ tesla}^2 \tag{A.3}$$

APPENDIX B

CALCULATION OF EJECTION CURRENT

The ejection pressure (P_{ej}) is proportional to the load current (I_1) and axial field (B_{ca}) as follows:

$$P_{ej} = \frac{B_{ca} I_1}{2\pi R_c} \tag{B.1}$$

The axial field due to the toroidal current is expressed as:

$$B_{ca} = \frac{\mu N I_1}{2\pi R_c} \tag{B.2}$$

where μ = permeability = $4\pi \times 10^{-7}$ (H/m)

N = number of drums = 4

R_c = collector radius = 0.1575 m

Thus, the ejection pressure becomes:

$$P_{ej} = \mu N \left(\frac{I_1}{2\pi R_c} \right)^2 = 5.13 \times 10^{-5} \, I_1^2 \tag{B.3}$$

The restoring pressure is expressed by:

$$P_{res} = \frac{\Delta h \rho V^2}{R_o} \tag{B.4}$$

where Δh = height differential (m)

ρ = NaK density = 850 (kg/m^3)

V = fluid velocity = 8.25×10^{-3} n (m/sec)

R_o = mean radius = $R_c - \frac{\Delta h}{2}$ (m)

In order to determine the restoring pressure (P_{res}) it is necessary to calculate the maximum head which can be produced just prior to ejection. It is assumed that the NaK can be pumped out to the point at which the trailing edge is even with the disk sidewall as shown in Figure B.1. The maximum height differential (Δh) will be a function of the liquid metal volume. The calculation of Δh is shown below for the 4 cc NaK case.

$$V_{TOTAL} = V_1 + V_2 + V_3 \tag{B.5}$$

$$V_1 = 2\pi R_c \, gW_d \tag{B.6}$$

$$V_2 = 2\pi R_c \, \Delta hx \tag{B.7}$$

$$V_3 = 2\pi R_c \left(\frac{\Delta h - 2.54\times10^{-3}}{2} \right)^2 \tag{B.8}$$

$$V_{TOTAL} = 2\pi R_c \left[\frac{\Delta h^2}{2} + (x - 2.54\times10^{-3})\Delta h + \frac{(2.54\times10^{-3})^2}{2} + gW_d \right] \tag{B.9}$$

$$4 \times 10^{-6} = 2\pi(0.1575) \left[\frac{\Delta h^2}{2} - 2.14\times10^{-3}\Delta h + 4.8\times10^{-6} \right] \tag{B.10}$$

$$\frac{\Delta h^2}{2} - 2.14 \times 10^{-3} \, \Delta h + 7.58 \times 10^{-7} = 0 \tag{B.11}$$

$$\Delta h = 3.89 \times 10^{-3} \text{ meters} \tag{B.12}$$

The restoring pressure thus becomes:

$$P_{res} = 1.45 \times 10^{-3} \, n^2 \tag{B.13}$$

Setting $P_{res} = P_{ej}$ and solving for ejection current:

$$I_{ej} = 16.8\ n \qquad \text{(B.14)}$$

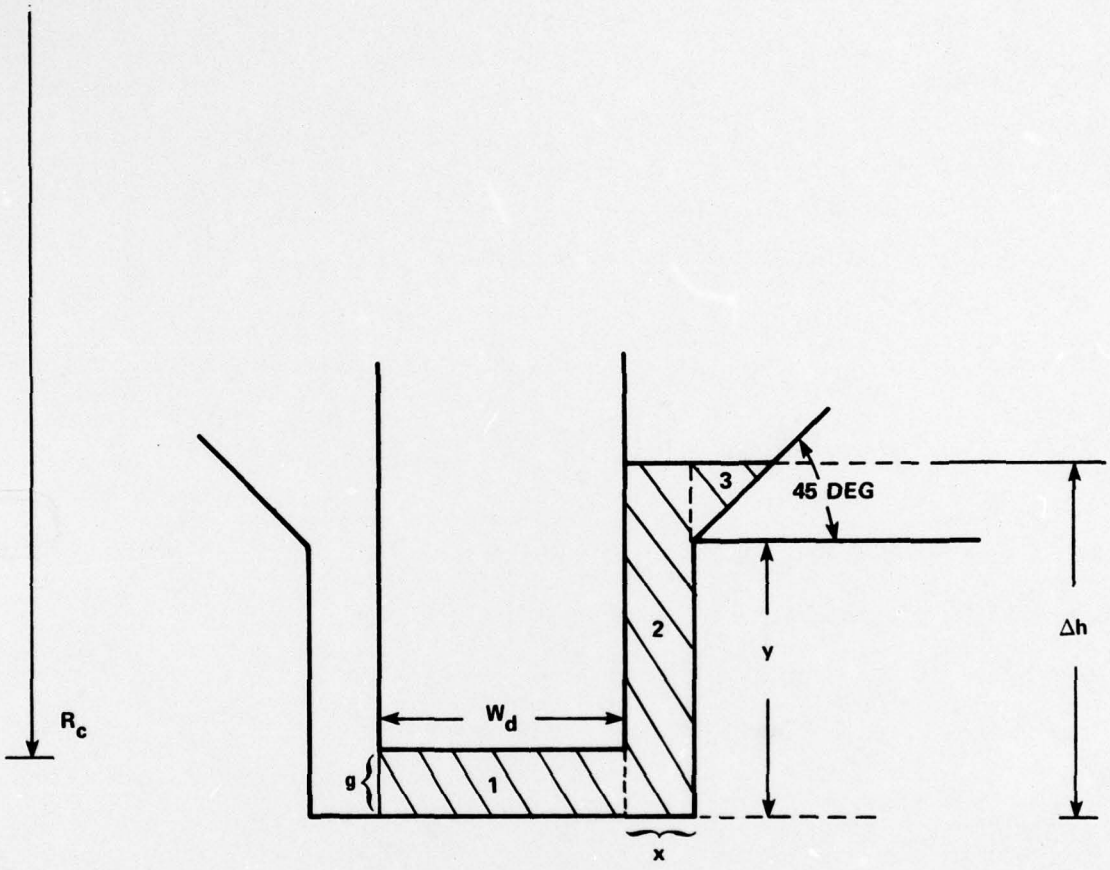

R_c = 0.1575 m
W_d = 0.00316 m
x = 0.0004 m
y = 0.00254 m
g = 0.0005 m

Figure B.1 - Model for Restoring Pressure Calculation

APPENDIX C

MOTOR NO-LOAD TEST PLAN

I Bearings, seals, windage losses (no NaK)

Q versus N (0, 300, 600, 900, 1200, 1500, 1800) $I_f = 0$ independent of I_f previously established

$\dot{w}_c = 8.5$

IIA Generator configuration with 2 cc NaK each site

V_T, Q versus N (0→1800) at I_f (0, 30, 60, 90, 120)

V_N (1→16) at N = 1800, $I_f = 120$

T_N (all) at N = 1800, $I_f = 120$

IIB Motor configuration with 2 cc NaK each site (disconnect coupling)

N versus V_T (6, 12, 18, 24, 30 volts) $N \leq 2400$ r/min at I_f (30, 60, 90, 120)

IIIA Generator configuration with 3 cc NaK each site

IIIB Motor configuration with 3 cc NaK each site

IVA Generator configuration with 4 cc NaK each site

IVB Motor configuration with 4 cc NaK each site

V Short circuit generator configuration at 4 cc NaK each site

Q versus N (600, 1200, 1800) at $I_f = 0+$

(Scope ΔV along terminal rods between sites)

T_N (all) at N = 1800 and maximum drive motor power

VI Short circuit generator configuration at 3 cc NaK each site

VII Short circuit generator configuration at 2 cc NaK each site

APPENDIX D

SUGGESTED MOTOR LOAD TEST PLAN

I Rectifier - motor configuration - no load

N versus V_T (0→30 volts): $N \leq 2400$ r/min

at I_f (30, 60, 90, 120)

IIA Rectifier - motor configuration - high current and low speed at 4 cc per site:

- constant voltage on power supply
- at nominal I_f set N, I_1
- decrease I_f while increasing I_1 to maintain N
- record I_1 ($\leq$ 10,000 amp) versus N (0→600 r/min)

IIB Same as IIA at 5 cc per site

IIC Locked rotor test at 4 cc and 5 cc per site

IIIA Rectifier - motor - dynamometer configuration at 4 cc per site:

- set I_f (30, 60, 90, 120); V_T (0→30 volts)
- set water level in dynamometer to determine load
- increase I_1 to maintain N
- record N ($\leq$ 2400 r/min), I_1 ($\leq$ 10,000 amp); Q; T (°F)

IIIB Same as IIIA at 5 cc per site

REFERENCES

1. Cannell, M.J. and T.J. Doyle, "Development of the Shaped Field Superconductive Motor," Naval Ship Research and Development Center Report 4178 (Jan 1974).

2. Doyle, T.J., "Superconductive Propulsion Motor Development at NSRDC," Naval Ship Research and Development Center paper presented at San Francisco, Inter-Society Energy Conservation Engineering Conference (28 Aug 1974).

3. Dunnington, R., "Liquid Metal Current Collector Development," Naval Ship Research and Development Center Report 27-580 (Oct 1974).

4. Rhodenizer, R.L., "Development of Solid and/or Liquid Metal Collectors for Acyclic Machines," General Electric Co., Corporate Research and Development Center Report, NAVSHIPSYSCOM Contract N00024-68-C-5415, S-71-1110 (Sep 1970).

INITIAL DISTRIBUTION

Copies	
2	CNR 1 Code 211 1 Code 473
3	NAVSEASYSCOM 2 SEA 0331H 1 SEA 543
12	DDC
1	MIT Cambridge, Mass. 02139 Attn: Dr. J. Smith
1	AiResearch Manufacturing Co. 2525 West 190th Street Torrance, CA 90509 Attn: Mr. M. Calderon
1	A. Stewart Bradford Computer & Systems Inc. 7700 Broadway New York, NY 10019
1	General Electric Co. Corporate Research and Development P.O. Box 43 Schenectady, NY 12301 Attn: Mr. R.A. Marshall
1	Westinghouse Electric Corp. Research Laboratories 130 Beulah Road Pittsburgh, PA 15235 Attn: Dr. D. Green

Copies	Code	Name
10	5211.1	Reports Distribution
1	522.1	Unclassified Lib (C)
1	522.2	Unclassified Lib (A)
2	5231	Office Services (A)

CENTER DISTRIBUTION

Copies	Code	Name
1	272	E. Quandt, Jr.
1	2703	W. Levedahl
5	2711	H. Robey
1	2771	W. Anderson